FU JEN STUDIES

NATURAL SCIENCES

NO. 20 1986

目 次 CONTENTS

Page

總統 蔣公科學思想言論選錄.....周 徵... 1
The Role of Science in the Thought of President Chiang Kai-shek: Selections from his Writings .....by *Chou Chung*

環狀糊精之研究 1. 性質、來源、生產及應用.....施能仁 丘志威... 7
Cyclodextrins: 1. Review of Recent Research Related to Properties, Sources, Production and Application .....
..... by *N.J. Shih* and *C.P. Chiu*

The Magnesium-DNA Binding Problem——A Dilution Study....
.....by *Elizabeth H. Mei*...15
用鎂 (25) 磁場共振方法來觀察錯離子在水溶液中的結合：
DNA-鎂鹽.....梅宏綺

^{25}Mg NMR the Magnesium-ATP Interaction——A Multinuclear NMR Study .....by *Elizabeth H. Mei*...25
用鎂 (25) 磁場共振方法來觀察錯離子在水溶液中的結合：
ATP-鎂鹽.....梅宏綺

續 (Continue)

FU JEN CATHOLIC UNIVERSITY

TAIPEI, TAIWAN, REPUBLIC OF CHINA

3

目　次（續） CONTENTS (continued)

Page

比較兩常用聚合物分子量分散率之測定.....陳天鐸　陳壽椿...33
Comparison of Two Popular Universal Calibration Methods for Polydispersity Determination by Gel Permeation Chromatography...by *Tain-Dow Chen* and *Show-Chuen Chen*

銅及銀離子選擇電極之改進.....饒忠儒　李榮忠　陳壽椿...43
The Improvements of Copper Ion and Silver Ion Selective Electrodes.....by *Jong-Ru Rau, Rong-Jong Lii* and *Show-Chuen Chen*

The Fine Structure of the Gill Filament in *Gomphina Veneriformis* Lamark.....by *Wen-Huei T'sui*...57
花蜊之組織及病理研究.....崔文慧

葡萄酵素性褐變之研究　II. 金香葡萄於發育與成熟過程中聚酚氧化酶活性之變化.....陳雪娥　金蘭馨...79
Studies on the Enzymatic Browning Capacity of Grapes II. Changes in Polyphenol Oxidase Activities during Development and Maturation of Golden Muscat Grape.....by *Hsueh-Err Chen* and *Lan-Shin Chin*

Abstracts of Papers by Faculty Members of the College of Science and Engineering that Appeared in Other Journals during the 1985 Academic Year.....85

中文 (1)

總統　蔣公科學思想言論選錄

理工暨外語學院共同科目

周　　徵

摘　　要

本校理工學院推展科學教育不遺餘力，除了在經費極端拮据之下，添置儀器設備之外，更爲中國科學教育尋根覓源。進而與西方科學術接結合，以期鞏固中國科學教育之穩定與發展，爲此更配合教育部科學教育政策，將　蔣公一生科學思想之言論，精心選錄，發交各學系研究實踐，以深入現行科學教育之中，形成一個正確的精神指標，可說是用心良苦，意行可欽。

值茲理工學院輔仁學誌刊物發刊之際，柏院長又特囑將「蔣公科學思想言論選錄」，刊爲卷首，以廣流傳，隨時惕勵，並囑爲文推介，以昭鄭重。

蔣公生前曾一再指出：

『科學發展之目的爲建設三民主義的現代化國家。其方針爲發展經濟、改善民生、開發國家資源、增進科學知識與技能，建立現代化健全政府與社會。』

謹將　蔣公思想言論，有關科學部份，恭錄如下，以茲惕勵。

一、科學的涵義

㈠什麼是科學：

1. 凡是知識之有系統的分析。而能歸納之於原理等。都可以叫做科學。（空軍救國三唯論）
2. 窮理致知。致知在格物。……即物窮理。事窮理以致其知。（科學的道理）
3. 本末始終與先後順序的學問。（新軍人倫理觀念）

㈡科學之條件：

1. 發揮我們聰明才知來認識宇宙，宰制宇宙，征服自然，利用自然。（中國青年之責任）
2. 將知識構成意像，將意像生出條理。本條理籌備計劃，按計劃去用功夫，則指日可望樂成也。
3. 練習、試驗、探索、冒險。即不知亦能。……這就是知難行易的道理。（心理建設之要義）
4. 科學上是求精密、求正確、求實在、求徹底。（軍事教育之檢討）

㈢科學的分類：

1. 聲光電化動潛植礦。都是自然事物爲研究對象，即自然科學。（大學之道）

2. 大學格物之物，乃是指一切具體的物與抽象的事而言。（大學之道）
3. 科學也有有形科學與無形科學之分。（三軍官校畢業典禮訓詞）

㈣科學的目的：

1. 格物致知，求及眞理眞知，止於至善。（大學之道）
2. 所謂利用天然者。一方面消極的適應天然。一方面積極的克服天然。一方面利用人類本能達成教育目的。一方面利用宇宙之本能增進人生之福利。（中國經濟學說）
3. 唯其理有未窮，致其知有未盡。（軍事教育目的與宗旨）
4. 科學卽正德利用厚生之道。（文化堂落成紀念文）

二、科學的方法

㈠什麼是科學方法：

1. 物有本末，事有終始，知所先後，則近道矣。（革命哲學的重要）
2. 知止而後有定，定而後能靜，靜而後能安，安而後能慮，慮而後得。以達止於至善之目的。（革命哲學）
3. 人類心智上的活動包括以下的要目：
   ⑴觀察與試驗。
   ⑵分析與綜合。
   ⑶想像推測理想化。
   ⑷推論。
   ⑸比較類推。
   （行政管理重要性）

三、科學的辦事方法

㈠辦事除了要講究組織、系統、範圍之外還要注意分析與歸納。

㈡無論做什麼事一定要四到：

1. 要心到——專心注意
2. 要口到——解析清楚
3. 要眼到——親自檢查
4. 要手到——親手督導（軍事教育要點）

㈢辦事之順序要由近而遠，自卑而高。爲大於微，圖强於易。（科學的道理）

㈣實事求是，精益求精，繼續不斷，貫徹始終，就是科學精神。（科學的道理）

㈤基本科學方法與程序：

1. 範圍與組織——凡事先認清範圍，……然後確定有力之組織，完成事功。
2. 立案與預備——將對象深入研究擬出計劃，假設數種情況，備妥數種方案。

3. 分工合作
4. 研究實驗——日新又新
5. 分析統計——經驗累積
6. 改進發明——精益求精（科學的道理）

㈥力行的法則：

1. 起點
2. 順序——系統、條理、計畫。
3. 目的
4. 恒久（行的道理）

㈦行政三聯制：

設計、執行、考核。詳細一點分、即爲：

1. 調查審核。　2. 檢討研究。
3. 設計步驟。　4. 決定實施。
5. 標準期限。　6. 順序分類。
7. 考驗評定。　8. 核實獎懲。

㈧其精神即爲：

有恒、實踐、合作、貫徹。

（工作要領與努力方向）

㈨科學的研究方法：

1. 研究方法

(1)環境與內容——先瞭解其客觀環境及其主要內容，才能透徹全局，然後因事因人因地因時而制宜。

(2)因果與法則——查其因推其果，其因果關係之發展法則，掌握其法則。

(3)理論與實踐——建立理論，身體力行。

（訓練之目的與實施綱要）

四、科學的精神

㈠存疑與創新

㈡分工與合作

㈢精益求精，實事求是。

㈣客觀與合理——窮理於事物始生之處。
研幾於心意初動之時。

㈤確實與徹底

㈥科學與哲學

1. 科學是思惟、法則、作爲、據依。重物質。

2. 哲學是智慧、意志、決心、判斷。重精神。

(七)科學與倫理：

1. 格物、致知、誠意、正心、修身、齊家、治國、平天下。——格物致知爲科學。
2. 誠意、正心，爲倫理基礎。
3. 修身、齊家，爲倫理道德。
4. 治國平天下爲倫理之目的。

(八)科學與宗教：

愛因斯坦說：『不論科學如何發達，總跳不出道德社會和精神生活，因爲我們對科學已走上身外的自然律，應當回頭來尋找我們內心的生命法。』——自然規律之結構，卽宗教情緒。內心生命卽宗教。（耶穌受難節證詞）

(九)科學與政治：

政治是個行政組織，要想發揮其所能，必須科學方法組織、科學的管理、科的處事方法、科學的研究改進、……才能奏功。（行政人員需知）

五、科學之發展

中國大學之道，卽爲教育訓練做人做事之基本法則。（軍事教育之宗旨）

中國大學中庸是中國正統哲學，也開科學之先河，今日物理科學，皆不能超越他。（大學之道）

(一)大學的科學精神與方法：

1. 卽物窮理
2. 研究預備
3. 分工合作
4. 精確眞實
5. 條理系統
6. 自强不息（爲學辦事做人基本要道）

(二)科學發展之方向：

1. 發揮我固有之知能
2. 吸收近代科學技術（建國運動）
3. 民生主義以科學爲基礎（三民主義本質）

(三)科學發展之方法：

1. 目的——建設三民主義現代化中國。
2. 方針——發展經濟，改善民生，開發資源，增進科技。
3. 途徑——加强科學教育，科學研究。
4. 科目——充實數理生化，基本科學，更以數學爲首要。

理工科應以電子、機械、原子、太空科學爲重。

海洋學、地質學、礦冶學、土木工程，亦應特別注意。

㈣科學發展之重點：

1. 行政院科學委員會，易名國家科學技術委員會，改爲首長制。
2. 人文社會科學部份並重。
3. 科學專門人才之培育與羅致當務之急。
4. 經濟部重在研究發展。
5. 科技分政府研究機構、各校研究所、民間研究部門，密切聯繫，以收分工合作之效。（考察韓日科技報告之指示）

㈤幹部之缺點：

1. 散漫零亂
2. 含混籠統
3. 舍本逐末
4. 粗枝大葉
5. 推諉拖延
6. 陽奉陰違（幹部教育之回顧）

此均缺乏科學概念及科學管理之故。

㈥工業社會之特點即科學精神：

1. 重對象
2. 求眞像
3. 求合理
4. 求進步
5. 求發展
6. 重客觀（幹部教育之回顧）

㈦所謂現代化，亦即綜合科學化、組織化，只是現代化具有比科學化更爲廣泛積極之意義。（軍事教育提示）

㈧全面革新，就是科學精神貫徹上下，做到新、速、實、簡。(全面革新之精神)

㈨科學建國，就是要先使我們精神、思想、觀念、行動、計劃、作爲，都合乎科學精神與方法。（科學的道德）

㈩講革新首要講求科學知識與方法。（革命歷史之啓示）

The Role of Science in the Thought of President Chiang Kai-shek: Selections from his Writings

CHOU CHUNG

Core Curriculum, College of Science and Engineering
and College of Foreign Languages

ABSTRACT

1986 is the one hundreth anniversary of the birth of the first president of the Republic of China, Chiang Kai-shek. President Chiang, together with the other founding Fathers of the Republic, saw empirical science, both its method of critical inquiry and its technological innovations, as critical to the development of the nation. At the same time they recognized the importance of preserving and enhancing the traditional values of Chinese society. As both a commemoration of the late President and an encouragement to further scholarly study, Professor Choe Chen, Professor of Modern Chinese History in the core curriculum of the College of Science and Engineering and the College of Foreign Languages, has provided us with excerpts from the writings of President Chiang on the topic of the role of modern science in China.

環狀糊精之研究

1. 性質、來源、生產及應用

食品營養系暨研究所

施能仁　丘志威

摘　要

本篇綜合近十幾年來有關環狀糊精的學術報告就環狀糊精的性質、來源、生產及應用作一詳細的回顧。此外，並介紹國內環狀糊精的研究近況。

自 Villers 氏於1891年發現環狀糊精 (cyclodextrins, 以下簡稱環糊精) 以來經過 Schardinger, Tilden, 及 French 等學者的研究，環糊精的性質乃被世人了解，並引起許多與環糊精相關的研究。

環糊精又名 Schardinger dextrins，環狀顆粒澱粉 (cycloamyloses) 或環狀葡聚糖 (cycloglucans)。環糊精爲數個葡萄糖以 α-1, 4 glycosidic linkage 所結合成的環狀寡糖類，其中 α-, β- 及 γ-環糊精分別指每環由 6，7 及 8 個葡萄糖基所組成的環糊精[11,13,53]。此外 δ-, ε-, ζ- 及 η-環糊精爲帶有分岐的環糊精，或由 9 個葡萄糖所聚合的環糊精[15,47]。

環糊精的性質

一般而言。環糊精具有下列性質：㈠不具有還原端及非還原端，使用過碘酸氧化時不會產生甲酸及甲醛[12]。㈡比澱粉較耐酸水解，且在碱液中不產生裂解現象[19]。㈢可與有機溶劑或油性物質形成包接化合物 (inclusion complex)。及㈣不具毒性，可應用於食品中。

α-, β- 及 γ-環糊精之性質亦互有差異。如表 1 所示：β-環糊精之溶解度較 α- 及 γ-環糊精低。在濾紙上與碘蒸氣作用後呈黃色，是環糊精中最易結晶純化者[34]。分岐型環糊精之溶解度均大於非分岐型環糊精[1,37]。

環糊精對於各種澱粉酶的抵抗力亦有所不同。外切型澱粉酶如 amyloglucosidase[29,30], β-amylase[55] 及 pullulanlase[43] 等分解環糊精均十分困難。而內切型澱粉酶如 Taka-amylase (*Aspergillus oryzae* amylase) 則可分解環糊精[17,21,29,52]，但對於分岐型 α- 環糊精則很難分解[36]。人體的澱粉酶無法水解環糊精，但位於大腸中的細菌 (*Bacteroides* strain) 可以將環糊精分解[2]。

表1. α-, β-, γ-[a] 環糊精及分岐環糊精的物理性質

	α-CD	β-CD	γ-CD	G•α-CD	G•β-CD
Number of glucose residues per ring	6	7	8	6	8
Cavity diameter (Å)	6-7	7-8	9-10	NM[b]	NM
Solubility (g/100 ml H_2O, 25°C)	14.5	1.85	23.2	>100	>15
$[\alpha]_D^{25}$ (in H_2O)	+155.5	+162.5	+177.5	NM	+178
Crystal form (in H_2O)	Needle	Prism	Prism	Needle	NM
Complex color with iodine	Blue	Yellow	Orange	Brown-purple	NM

a: α-CD: α-cyclodextrin; β-CD: β-cyclodextrin; γ-CD: γ-cyclodextrin; G•α-CD: 6-0-α-D-glucosyl-α-cyclodextrin; G•β-CD: 6-0-α-D-glucosyl-β-cyclodextrin.

b: Not mentioned.

Source: Kobayashi *et al.*(37), Kobayashi and Kainuma(34) and Abe *et al.*(1).

表2. 環糊精葡萄糖基轉移酶的性質

Bactəria spieces	Optimun pH	pH stability	Optimun temperature °C	Heat stability (°C) w/o Ca++	Heat stability (°C) with Ca++	Major yield of CD[a]	Yield %
Bacillus macerans	5.2-5.7	8.0-10.0	55-56	50	60	α-CD	50-60
Bacillus megaterium	5.0-5.7	7.0-10.0	55	55	NM[b]	β-CD	NM
Bacillus stearothermophilus	6.0	7.0-9.2	70	50	NM	α-CD	45
Bacillus circulans	5.2-5.7	7.5-9.0	55	50	NM	β-CD	NM
Alkalophilic *Bacillus* sp.	4.5-9.0	6-10	45-50	65	70	β-CD	75-85
Klebsiella pneumoniae	5.3	6.0-7.5	NM	NM	45	α-CD	50

a: CD stands for cyclodextrin.

b: Not mentioned

Source: Horikoshi(19).

環糊精之來源及生產

自 Kerr 提出環糊精是澱粉中之一部份假說以來[22]，經無數研究，才證明環糊精爲澱粉經環糊精葡萄糖基轉移酶(cyclodextrin glycosyltransferase，簡稱 CGTase) 作用而來。CGTase 早期發現於 *B. macerans*[9,10,33,51,56,57]，所以又稱爲 *B. macerans* amylase (BMA)。目前除了 *B. macerans* 之外，CGTase 亦可在 *B. megatersum*[24], *B. circulans*, *B. stearothermophilus*[28], alkalophilic *Bacillus* 及 *K. pneumoniae* 等 5 種菌株找到。不同菌株所產的環糊精量及種類亦不一樣。表 2 列舉了一些 CGTase 的特性。CGTase 除了存在菌體內，亦存在於菌體外[8,51]。

CGTase 主要參與的反應有 3 種：㈠環化作用。可將澱粉由非還原端切成環糊精[22,31,35]，㈡偶合反應 (coupling reaction)。有接受糖 (acceptor sugar) 存在時，CGTase 可將環糊精水解，再接於接受糖之非還原端上[3,5,8,14,16,18,23,25,26,31,35]，此作用以 *B. megaterium* 之 CGTase 爲最明顯[18]，㈢醣鏈長短互換作用 (disproportionation)。兩條醣鏈 (saccharide) 可以彼此交換葡萄糖基而增加或減少醣鏈的長度[34]。

許多研究報告指出：alkalophilic *Bacillus* 所產的 CGTase 最適合生產環糊精[19,20,40,44]。圖 1 詳列目前工業界製造環糊精的流程；於 85°C 將含有 10mM $CaCl_2$, CGTase 及 pH 6～9 之15%馬鈴薯澱粉懸浮液液化30分鐘，隨即降溫至 55°C，並調 pH 值至8.5。再加入 CGTase 進行環化作用 24～44 小時。再加熱至 100～120°C 使 CGTase 失去活性。將反應液調至 pH 6～7 後加入 α-amylase 以去除未反應的醣，再經活性碳脫色，陰陽離子交換樹脂去除離子後，於 60°C 減壓濃縮至 45～50 Brix。濃縮液經水冷過夜 (25°C)，離心後，可得 β-環糊精結晶及含有 α- 及 γ-環糊精之糖漿。

最近，由於薄膜技術 (membrane technology) 的發展，因此亦可以利用薄膜技術來生產環糊精。Kobayashi 等[36] 曾使用薄膜技術來生產環糊精。如圖 2 所示：將液化澱粉與 CGTase進行環化反應後，利用超濾(ultrafiltration) 將小分子的環糊精濾出，而未被濾出之 CGTase 及液化澱粉則可再次反應形成環糊精。經過超濾後所得含有環糊精的液體再由逆透膜 (reversible osmosis) 進行濃縮。將濃縮液置於結晶槽中，使 β-環糊精結晶，因而可得含有 α-，γ-環糊精之糖漿及 β-環糊精結晶。

由於 CGTase 爲一昂貴的酵素來源，因此使用 CGTase 將澱粉液化步驟可使用鹽酸浸漬法或 α-amylase 液化法來減少 CGTase 的使用量，但效果並不如直接使用 CGTase 液化來得好[54]。此外，亦可將 CGTase 進行固定化[60]以減少酵素的消耗。

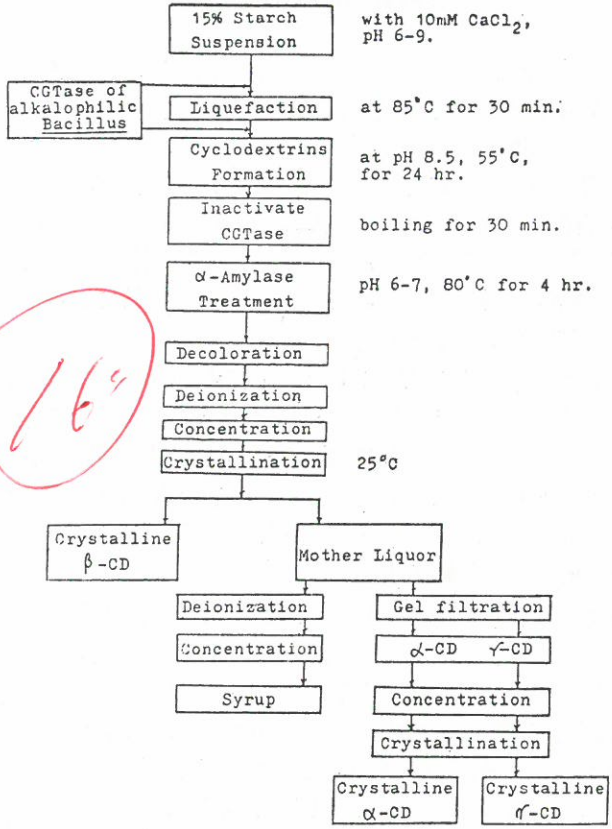

Source: Nakamura and Horikoshi[44].

圖 1. 使用環糊精葡萄糖基轉移酶生產環糊精之流程圖

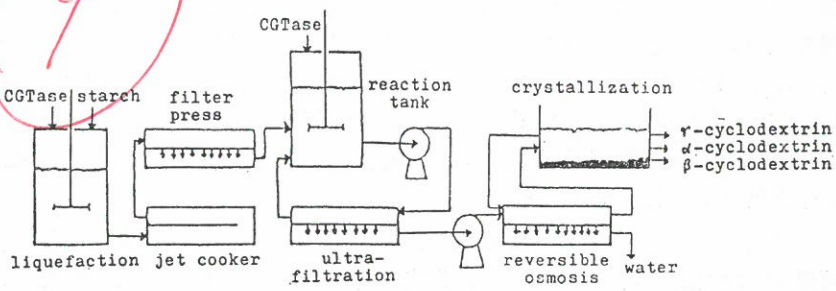

Source:Kobayashi *et al.*[86].

圖 2. 使用超濾及逆透膜生產環糊精

環糊精的生產受許多因子影響：㈠還原糖量。反應液中含有少量還原糖，則環糊精產量明顯減少[60]。這是因爲還原糖爲接受糖體，使 CGTase 進行偶合反應的緣故。㈡油脂含量。Wilson等[59]發現在反應液中加入1% oleic acid後，反應液中會增加雲狀物含量，由此可推論澱粉所含有的油脂會干擾 CGTase 的作用而減少環糊精產量。㈢澱粉濃度。在低濃度中，例如1%澱粉濃度，可以得到大約75～80%的環糊精產量，但過稀的澱粉濃度會造成生產上的浪費，因此工業界均使用15%澱粉濃度[20,34,40,44]。於此濃度下只能得到約 10～15%環糊精產量[40,44]。㈣緩衝溶液濃度。由於 CGTase 爲一種轉移酶，因此在較低濃度的緩衝溶液中，環糊精產量較高。但以馬鈴薯澱粉作原料，在 200 mM 醋酸鈉緩衝溶液（pH 6.9）中，經 *K. pneumoniae* 之 CGTase 作用後，所得的 γ-環糊精產量最高，此原因尚不十分明瞭[6]。㈤直鏈澱粉含量，直鏈及分岐澱粉經 *B. macerans* CGTase 作用後，分別得到70%及50%環糊精[59]，由此可見直鏈澱粉含量高的澱粉具有較高環糊精產量。CGTase 作用在分岐澱粉之A鏈上面，B鏈之環糊精產量則十分稀少[4,7]。㈥界面活性劑。添加不同種類界面活性劑均可增加環糊精產量。其中 6_5 helix 型直鏈的界面活性劑如 SDS 可增加 α-環糊精產量，却抑制 β- 及 γ-環糊精產量[32,37]。而帶有苯環基 7_6 helix 型界面活性劑，如 Triton，却增加 β-環糊精產量[14]。

環糊精之應用

環糊精由於其特殊的環形排列，如圖 3 使得內部爲疏水性，外部爲親水性，所以很容易與油溶性物質形成包接化合物（inclusion complex）。目前環糊精的應用均以 β-環糊精爲主。有關環糊精應用的文獻則多限於專利方面。

Nakamura Horikoshi[44]曾針對環糊精之性質推測環糊精可應用在醫藥、食品、化粧品及殺蟲劑等方面。環糊精可作爲藥品的安定劑及保存劑，增加藥品的溶解度及去除藥品的苦味。在食品方面，添加 0.3 至 0.5% β-環糊精於柑橘果汁中，可以去除 naringin 及 limonin 所引起之苦味及防止因 hesperidine 引起的果汁沉澱[38,39,41]。而果汁中之固形物，總酸量及維生素C並不受添加 β-環糊精的影響[48,49]。

Linder 曾說明環糊精在茶點中應用的可行性[42]。此外環糊精亦可作爲油脂抗氧化劑[50]色素安定劑[2]、及增加維生素A、D、E、K的溶解度[46]。添加環糊精的香水，化粧品可防止香氣的散失而增加使用期限[19]。

國內環糊精的研究

大同工學院於民國72年開始研究製造環糊精的可行性，目前已設立實驗工廠進行小量 β-環糊精的生產。輔仁大學食品營養研究所於民國 73 年開始研究由不

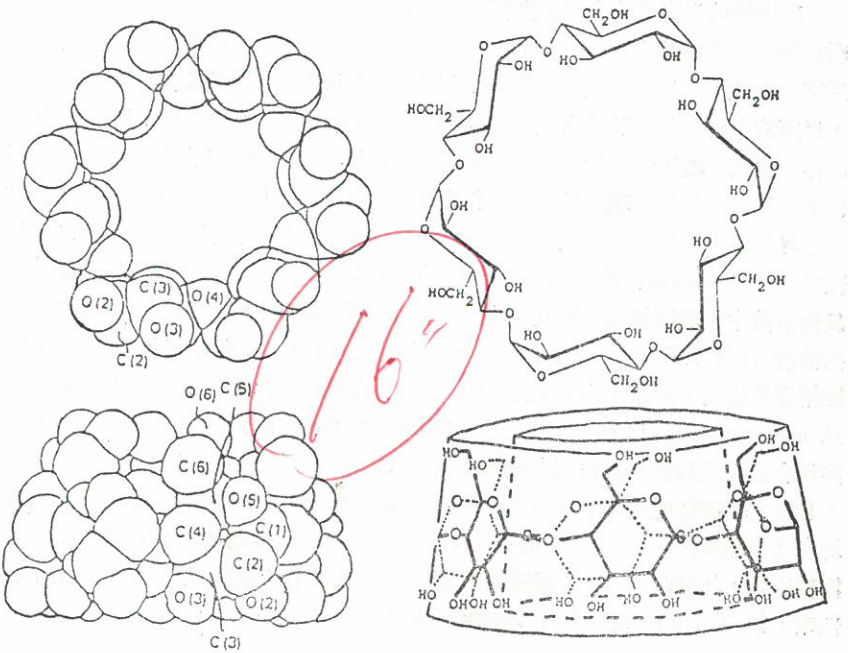

Source: Nakamura and Horikoshi[44] and Tu *et al.*[58].

圖 3. α-環糊精之分子模型

同澱粉生產環糊精的可行性，並繼續探討 α-, β-, γ-環糊精的分離純化及環糊精甲基化或羧甲基化以提高溶解度之技術。國立臺灣大學農化系及榮民總醫院亦分別進行生產環糊精酵素性質及製藥應用等方面之研究。雖然環糊精在國內的研究歷史不算長，但是在民間廠商及國科會有計畫的推動下，環糊精的發展潛力應是相當樂觀的。

參 考 文 獻

(1) J. Abe, Y. Taketa, S. Hizukuri, K. Yamashita and N. Ide, *Carbohydr. Res.* **131**, 175 (1984).
(2) R. N. Antenucci and J. K. Palmer, *J. Agric. Food Chem.* **32**, 1316 (1984).
(3) H. Bender, *Carbohydr. Res.* **101**, 279 (1982).
(4) H. Bender, *Carbohydr. Res.* **110**, 245 (1982).
(5) H. Bender, *Carbohydr. Res.* **117**, 1 (1983).
(6) H. Bender, *Carbohydr. Res.* **124**, 225 (1983).
(7) H. Bender, *Stärke* **36**, 46 (1984).
(8) J. A. DePinto and L. L. Campbell, *Science* **146**, 1064 (1964).
(9) J. A. DePinto and L. L. Campbell, *Biochem.* **7**, 114 (1968).

(10) J. A. DePinto and L. L. Campbell, *Arch. Biochem. Biophys.* **125**, 253 (1968).
(11) D. French and R. E. Rundle, *J. Am. Chem. Soc.* **64**, 1651 (1942).
(12) D. French and R. L. McIntire, *J. Am. Chem. Soc.* **70**, 3145 (1950).
(13) D. French, D. W. Knapp and J. H. Pazur, *J. Am. Chem. Soc.* **72**, 5150 (1950).
(14) D. French, M. L. Levice, E. Norberg, P. Nordin, J. H. Pazur and G. M. Wild, *J. Am. Chem. Soc.* **76**, 2387 (1954).
(15) D. French, A. O. Pulley, J. A. Effenberger, M. A. Rougvine and M. Abdullah, *Arch. Biochem. Biophys.* **111**, 153 (1965).
(16) D. French, J. H. Pazur, M. L. Levine and E. Norberg, *J. Am. Chem. Soc.* **70**, 3145 (1984).
(17) V. M. Hanrahan and M. L. Caldwell, *J. Am. Chem. Soc.* **75**, 2191 (1953).
(18) E. J. Heher, K. Mizokami and S. Kitahata, *J. Jpn. Soc. Starch Sci.* **30**, 76 (1983).
(19) K. Horikoshi, *Process Biochem.* **14**(3), 26 (1979).
(29) K. Horikoshi, N. Nakamura, N. Matsuzawa and M. Yamamoto, *Int. Sym. on Cyclodextrins.* p. 25, Bundepest (1981).
(21) I. Joda'l, L. Kandra, J. Harangi, P. N'an'asi and J. Szejtli, *Stärke* **36**, 140 (1984).
(22) R. W. Kerr, *J. Am. Chem. Soc.* **65**, 188 (1943).
(23) S. Kitahata and S. Okada, *Agric. Biol. Chem.* **39**, 2185 (1975).
(24) S. Kitahata, N. Tsuyama and S. Okada, *Agric. Biol. Chem.* **38**, 387 (1974).
(25) S. Kitahata and S. Okada, *J. Biochem.* **79**, 641 (1976).
(26) S. Kitahata and S. Okada, *Agric. Biol. Chem.* **42**, 2369 (1978).
(27) S. Kitahata and S. Okada, *J. Jpn. Soc. Starch Sci.* **29**, 13 (1982).
(28) S. Kitahata and S. Osaka, *J. Jpn. Soc. Starch Sci.* **29**, 7 (1982).
(29) S. Kobayashi, K. Kaimura and S. Suzuki, *J. Jpn. Soc. Starch Sci.* **21**, 131 (1974).
(30) S. Kobayashi, K. Kaimura and S. Suzuki, *J. Jpn. Soc. Starch Chem.* **22**, 6 (1975).
(31) S. Kobayash, *J. Jpn. Soc. Starch Sci.* **22**, 126 (1975).
(32) S. Kobayashi, K. Kaimura and S. Suzuki, *J. Agric. Chem. Soc. Jpn.* **51**, 691 (1977).
(33) S. Kobayashi, K. Kaimura and S. Suzuki, *Carbohydr. Res.* **61**, 229 (1978).
(34) S. Kobayashi and K. Kaimura, *Fermentation and Industry* **36**, 176 (1978).
(35) S. Kobayashi, K. Kaimura and French, *J. Jpn. Soc. Starch Sci.* **30**, 62 (1983).
(36) S. Kobayashi, K. Maruyama and K. Kaimura, *J. Jpn. Soc. Starch Sci.* **30**, 231 (1983).
(37) S. Kobayashi, W. Shibiya, B. M. Young and D. French, *Carbohydr. Res.* **126**, 215 (1984).
(38) A. Konno, M. Miyawaki, M. Misaki and K. Yasumashu, *Agric. Biol. Chem.* **45**, 2341 (1982).
(39) A. Konno, M. Misaki, J. Toda, T. Wada and K. Yasumashu, *Agric.* Biol. *Chem.* **46**, 2203 (1982).
(40) M. Matsuzawa, M. Kawano, N. Nakamura and K. Horikoshi, *Stärke* **27**, 410 (1975).
(41) M. Misaki, *J. Jpn. Soc. Starch Sci.* **31**, 98 (1984).

(42) K. Linder, *Nahrung* **26**, 675. (In *Food Sci. and Technol. Abstr.* **15**, 2783 (1982).
(43) J. J. Marshall, *FEBS Letters* 37, 269 (1973).
(44) N. Nakamura and K. Horikoshi, *Chem. Econ. Eng. Rev.* 14(9), 32 (1982).
(45) E. Norberg and D. French, *J. Am. Chem. Soc.* **72**, 1202 (1950).
(46) J. Pitha, *Life Sci.* 29, 307 (1981).
(47) A. O. Pulley and D. French, *Biochem. Biophys. Res. Commun.* **5**, 11 (1950).
(48) P. E. Shaw and C. M. Wilson, *J. Food Sci.* 48, 646 (1983).
(49) P. E. Shaw, J. H. Tatum and C. M. Wilson, *J. Agric. Food Sci.* **32**, 832 (1984).
(50) H. Shlenk, D. M. Sand and J. A. Tillotson, *J. Am. Chem. Soc.* **77**, 3587 (1955).
(51) A. Stavn and P. E. Granum, *Carbohydr. Res.* **75**, 243 (1979).
(52) N. Suetsugu, S. Koyama, K. Takeo and Kuge, *J. Biochem.* **76**, 57 (1974).
(53) K. Takeo and T. Kuge, *Agric. Biol. Chem.* **33**, 1174 (1969).
(54) C. P. Tang and G. O. Lei, *Tatung J.* **14**, 85 (1984).
(55) J. A. Thoma and D. E. Koshland, *J. Am. Chem. Soc.* **82**, 3329 (1960).
(56) E. B. Tilden and C. S. Hudson, *J. Am. Chem. Soc.* **61**, 2900 (1939).
(57) E. B. Tilden and C. S. Hudson, *J. Bacteriol.* **43**, 527 (1942).
(58) A. T. Tu, J. Lee and F. P. Milanovich, *Carbohydr. Res.* **76**, 239 (1979).
(59) E. J. Wilson, T. J. Shock and C. S. Hudson, *J. Am. Chem. Soc.* **65**, 1207 (1943).
(60) C. P. Yang and C. H. Hung, *Tatung J.* **14**, 95 (1984).

Cyclodextrins: 1. Review of Recent Research Related to Properties, Sources, Production and Application

N. J. SHIH and C. P. CHIU

Graduate Institute of Nutrition and Food Science

ABSTRACT

The cyclodextrins is reviewed. A brief discussion of cyclodextrins properties, sources, production and application is presented. Because of the increased interest in this research, some recent research areas in Taiwan are described also.

THE MAGNESIUM-DNA BINDING PROBLEM

A Dilution Study

ELIZABETH H. MEI*

Department of Chemistry, University of Minnesota

ABSTRACT

The magnesium-25 NMR line widths are followed as a function of the solute concentration in aqueous solutions initially containing 80 mM magnesium chloride and 20 mM DNA phosphate both in the presence and absence of a high sodium chloride concentrations. The ^{25}Mg NMR line width is independent of concentration at low supporting electrolyte concentrations, but decreases in a manner consistent with a simple mass law binding reaction in high supporting electrolyte concentrations. This series of measurements demonstrates the modulation the counter ion binding equilibrium by the electrostatic part of the association.

INTRODUCTION

A number of features are involved in a detailed understanding of metal ion-macromolecule binding. Of particular interest is the relative importance of specific or chemically bonded interactions compared with non specific, longer range, electrostatic interactions.[1] We follow the suggestion of Manning[2] to take as specific interactions those that involve the first coordination sphere of the metal ion. By territorial binding we will include those interactions which at a minimum maintain the first coordination sphere hydration of the metal ion intact throughout the interation. DNA serves as a good model for a linear polyelectrolyte, though it clearly holds a wider fascination. Previous studies[3-5] have demonstrated that the ^{25}Mg NMR spectrum is influenced strongly by relatively slow chemical exchange reactions with DNA environments which is taken as primary evidence for the involvement of the magnesium ion first coordination sphere in at least some magnesium-DNA interactions.

* Current address: Elizabeth H. Mei, Ph. D., 842 Morningside Drive, Millbrae, CA 94030, U. S. A. Dr. Mei is an alumnus of Fu Jen Catholic University.

This conclusion is in constrast to that reached based on a kinetic argument advanced by Porschke.[6] Studies by Kearns[7-9] *et al.* exploiting paramagnetic divalent metal ions have led to the conclusions that about 15% of the bound divalent ions Mn^{2+} and Co^{2+} are involved in a first coordination sphere association. Though there is little reason to believe that the group IIA metal ions should be equivalent to the transition metal ions used in these studies, the result is not inconsistent with the ^{25}Mg data, the quantitative interpretation of which requires an assumption about the strength of the interaction driving the relaxation or the chemical exchange rate.[3]

The ^{25}Mg NMR data raises several questions about the extent of first coordination sphere vs territorial binding interactions. At high concentration of both DNA and magnesium, sodium and calcium ion are unable to titrate away much of the ^{25}Mg NMR line broadening. Previous experimental limitations prevented exploration of the ^{25}Mg NMR spectra at low concentrations though the NMR spectrum should reflect the difference between territorial and specifically bound structures. The approximate range for magnesium-phosphate association constants is known,[10] and is such that, in the absence of poly ion effects, the Mg-DNA complex should dissociate on dilution of both partners into the mM range. We report here the results of a dilution experiment carried out on magnesium-DNA solutions that demonstrates clearly the simultaneous importance of electrostatic and chemical interactions in this poly ion-divalent cation system.

The basis of the experiment is that, based on a growing library of experimental evidence from other nuclei[11-13] large effects on the quadrupole relaxed ^{25}Mg line widths should result only when the symmetry of the hexaaquo is lowered by disruption of the first coordination sphere. Thus, the ^{25}Mg NMR relaxation will be most sensitive to or largely dominated by the site specific interactions. The remaining longer range effects are expected to be similar to those found for ^{23}Na-DNA interactions,[14,15] i.e., several Hz, but not hundreds of Hz. We report here a pair of experiments that are elementary extensions of preuious work made possible by advances in instrumentation.

EXPERIMENTAL

The NMR spectrometer employed in these experiments was a Nicolet NT-300 operating with a 93 mm bore Oxford magnet and the standard Nicolet multinuclear low frequency probe. The magnesium-25 NMR line shape is known to be nonlorentzian, a problem that will be addressed elsewhere,[16] and the present report includes only the full line width measured at half maximum height. The experiments summarized in Fig. 1 were repeated three times on different samples and the errors in the line widths are at least 5% due to small fluctuations in the temperature and magnet homogeneity. Samples were contained in 15 mm NMR tubes and measured at

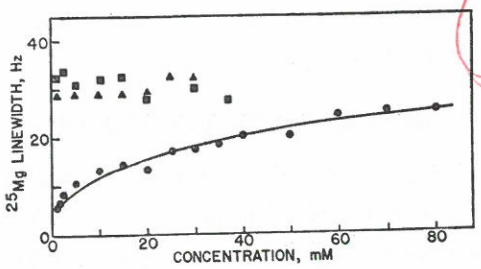

Fig. 1. The magnesium-25 NMR line width measured at 18.36 MHz for two types of DNA samples. (▲) The initial solution contained 40 mM $MgCl_2$ and 10 mM DNA phosphate and 10 mM NaCl. 10 mM NaCl was added as the diluent. (■) The initial solution contained only trace amounts of sodium chloride, 10 mM DNA phosphate, and 40 mM $MgCl_2$. Water was used as the diluent. (●) The initial solution contained 80 mM MgCla and 20 mM DNA and 1 M NaCl. The 1 M NaCl was used as the diluent. The solid line through the filled circles was calculated as described in the text based on a simple mass law binding interaction with an apparent equilibrium constant of 30 M^{-1}; however, as discussed in the text, this value may have no fundamental significance.

* Few data points in this figure are taken from Ms. S.H. Peterson's Master Degree thesis, University of Minnesota, Chemistry Department.

18.46 MHz. Temperature was controlled in the usual ways with a nitrogen gas stream.

The DNA used in this work was obtained from Millipore Corporation as the calf thymus preparation. The aqueous solution was sonicated ten times with 15 sec bursts at ~50 watt followed by 15 sec cycle with the power off, followed by 5 minutes of cooling. The above cycle was repeated 8 times. The DNA was characterized using Agarose gel electrophoresis to measure the average size of the product which was found to be 23 kilobase pairs. This product was dialyzed against EDTA to remove possible contaminant metal ions followed by extensive dialysis against water. This product was precipitated with absolute ethanol, centrifuged, lyophilized, and stored in the freezer until use. The NMR samples were prepared by weight and the final concentrations determined optically using a Cary 17 D spectrophotometer.

RESULTS AND DISCUSSION

The magnesium-25 NMR line width is shown in Fig. 1 plotted as a function of concentration for magnesium-DNA solutions in the presence and absence of a high supporting electrolyte concentration. In the first experiments shown by the solid triangles and squares, the magnesium-DNA sample was diluted with water. In the second experiment the electrolyte concentration was maintained with sodium chloride at 1.00 M throughout the dilution of the magnesium and DNA concentrations. In the first case no decrease in the magnesium-DNA interaction is reported by the NMR measurement, but in the second case thc decrease in the binding interaction is readily apparent.

The data qualitatively demonstrate the importance of the electrostatic and the chemical components of the overall binding. When the electrostatic contribution to the binding interaction is minimized by the addition of a high concentration of supporting electrolyte, the system behaves in the same was one expects for simple site binding. In the absence of the supporting electrolyte, the system behaves like the effective association constant is considerably higher,

presumably because the equilibrium between the magnesium ion and specific sites is buffered against the dilution of the bulk solute concentration because of the electrostatic concentration of the counter ion close to the macromolecule. It should be noted that the electrostatic contribution alone is inadequate for describing the NMR experiment as in that case the high concentrations of sodium ion or calcium ion used in this and previous experiments should displace virtually all of the bound magnesium ion,[3,4] which is not observed.

Quantitative interpretation is more difficult. The solid curve shown in Fig. 1 was calculated with the assumptions that the magnesium ion-DNA interaction could be described by a simple mass law association reaction involving equivalent and independent sites. With this very simplified model, the data are fit with an apparent equilibrium constant of $30\pm10\,M^{-1}$ and a line width for the bound environment of 120 Hz. Neither of these figures is in agreement with expectation and both are subject to critical evaluation.

Though there is considerable compensation between the line broadening parameter and the apparent equilibrium constant in the fitting precedure, the data are not consistent with an equilibrium constant considerably below $20\,M^{-1}$ or considerably greater than $40\,M^{-1}$. Nevertheless, even the smallest value is larger than our expectations for magnesium ion binding to an isolated phosphate diester group, though we are unaware of a really appropriate report on a model system. This large value may arise from several sources: 1) the electrolyte concentration may not be sufficiently high to eliminate all of the electrostatic contributions to the net binding interoction; 2) the bound environment may involve bidentate coordination of the metal ion; 3) the phosphate sites may not be independent. At 1.0 M the sodium ion concentration is sufficiently high that further decrease in the magnesium line width was not found with an increase in sodium concentration.[3-5] By this measure the concentration of the electrolyte should be high enough to minimize the importance of (1). The possibility of bidentate coordination is real and interesting, but we have no knowledge of what specifically this environment might be. Simple geometric considerations based on

the Watson-Crick double helix suggest that the distance between phosphate groups is too great for simultaneous first sphere coordination of a single magnesium ion to two phosphate oxygens without local denaturation or the participation of a bridging water molecule at one site.[6] The participation of nonphosphate donor atoms is also possible, but the present experiments do not provide a test of these possibilities.

An additional problem with the assumptions that lead to the solid curve in Fig. 1 is that at the highest concentrations shown, the equilibrium constant of $30\,M^{-1}$ predicts that the effective charge on the DNA will be positive rather than negative. Though evidence of charge reversal is difficult to obtain because of the nature of the solutions, we are unaware of unequivocal evidence that this is the case. An alternative is to assume that only some fraction of the phosphate groups is suited for the site specific association relaxation. For example decreasing the effective concentration of phosphate groups in the equilibrium expression by a factor of 10 drops the fraction of phosphate groups coordinated to magnesium from about 66% to 7% at the highest concentration of Fig. 1, which is not far from other estimates of the importance of site specific interaction[7,17] using similar metals. Though such as assumption may be reasonable, and is supported by previous work using paramagnetic metal ions, the present data are clearly not sufficient for a precise accounting of the number of phosphate groups involved in first coordination sphere bonds to magnesium ion.

The magnitude of the line width in the bound environment is obtained from several assumptions about the nature of the nuclear magnetic relaxation in the magnesium-DNA solutions. Though there are effects of nonextreme narrowing likely to be important in solutions such as these,[18] a simplified model is appropriate to this level of approximation. The observed line broadenining is then given by the elementary relation:

$$(\Delta\nu_{obs} - \Delta\nu_{control}) = P_b\,\Delta\nu_b \qquad (1)$$

where P_b is equal to the concentration of the magnesium-DNA

complex divided by the total magnesium ion concentration, and the bound line width is given by

$$\Delta\nu_b = \frac{1}{\pi}\left(\frac{1}{T_{2b} + \tau_{ex}}\right) \qquad (2)$$

The value of 120 Hz used in the calculation of the solid line in Fig. 1 curve B is surprisingly small given the relaxation rates for magnesium ion in complexes such as MgEDTA[19] or MgATP.[20] This figure cannot, therefore, reflect even a crude approximation to the bound relaxation rate, $1/T_{2b}$. As demonstrated previously, the metal-ligand exchange rate makes an important contribution to the line width in these solutions. Thus, equation 2 simplifies further to be directly a measure of the exchange rate. If all the phosphate groups are included in the interaction, this approach predicts a lifetime of 2.6 ms, which like the equilibrium parameter is large. If one decreases the effective concentration of phosphate groups that are uniquely suited to participate in the binding interaction, by a factor of 10, then the lifetime of the Mg-DNA interaction must be adjusted toward shorter times by a similar factor. A factor of 10 decrease in lifetime is more consistent with magnesium metal-ligand exchange kinetics. In any case it is important important to note that the lifetime of magnesium in the binding interactions monitored by the magnesium NMR is long, on the order of tenths of ms, many orders of magnitude longer than those characterizing the solvent separated interactions deduced for the hydrated alkali metal ions such as sodium ion[17] or reported for divalent ions using transient kinetic methods. It is interesting that the most reasonable interpretation of the ^{25}Mg data is consistent with the results of Kearns and Co workers for Mn^{2+} and Co^{2+} ions.

In summary these data provide evidence that a fruitful way to think of the divalent ion binding interaction with linear poly electrolytes is as the sum of contributions from the electrostatic concentration of ions at the poly ion surface and chemical or site specific interactions. These data suggest that the apparent equilibrium constant for the first coordination sphere binding is shifted by more

than an order of magnitude by the electrostatic contribution to the free energy. This sort of picture is often discussed and these effects separated in considerations of ion-membrane systems, which for present purposes are two dimensional rather than one dimensional poly ions.[21]

ACKNOWLEDGEMENTS

I would like to thank University of Minnesota, Chemistry Department for the use of NMR spectrometer and Prof. R.G. Bryant who initiated the project and support of this work from National Institutes of Health, GM-25757.

REFERENCES

(1) C.F. Anderson, M.T. Record, Jr., P.A. Hart, *Biophys. Chem.* **7**, 301 (1978).
(2) G.S. Manning: *Acc. Chem. Res.* **12**, 443 (1979).
(3) D.M. Rose, M.L. Bleam, M.T. Record, Jr., R.G. Bryant, *Proc. Natl. Acad. Sci. U.S.A.* **77**, 6289 (1980).
(4) D.M. Rose, C.F. Polnaszek, R.G. Bryant, *Biopolymers* **21**, 653 (1982).
(5) D.M. Rose, *Ph. D. Thesis*, University of Minnesota (1980).
(6) D. Pörschke, *Biophysical Chemistry* **4**, 383 (1976).
(7) J. Granot, J. Feigon, D.R. Kearn, *Biopolymers* **21**, 181 (1982).
(8) J. Granot, D.R. Kerans, *Biopolymers* **21**, 203 (1982).
(9) J. Granot, D.R. Kearns, *Biopolymers* **21**, 219 (1982).
(10) L.G. Sillen, A.E. Martell, *Stability Constants of Metal Ion Complexes* (Special Publication No. 17, 24, The Chemical Society, Burlington House, London 1964).
(11) K.D. Rose, R.G. Bryant, *J. Magn. Reson.* **35**, 223 (1979).
(12) J.G. Russell, R.G. Bryant, *J. Phys. Chem.*, Submitted.
(13) V.P. Chacko, R.G. Bryant, *J. Magn. Reson.*, Submitted.
(14) D.M. Rose, *Ph.D. Thesis*, University of Minnesota, Minneapolis, MN (1980).
(15) M.L. Bleam, C.F. Anderson, M.T. Record, Jr., *Proc. Natl. Acad. Sci. U.S.A.* **77**, 3085 (1980).
(16) E. Mei, C.F. Polnaszek, R.G. Bryant, Unpublished.
(17) C.F. Anderson, M.T. Record, Jr., *Ann. Rev. Phys. Chem.* **33**, 191 (1982).
(18) T.E. Bull, S. Forsen, D.L. Turner, *J. Chem. Phys.* **70**, 3106 (1979).
(19) E. Bouhoutsos-Brown, D.M. Rose, R.G. Bryant, *J. Inorg. Nucl. Chem.* **43**, 2247 (1981).
(20) E. Mei, R.G. Bryant, unpublished and R.G. Bryant, *J. Magn. Reson.* **6**, 159 (1972).
(21) S. McLaughlin, N. Mulrine, T. Gresalfi, G. Vaio, A. McLaughlin, *J. Gen. Physiol.* **77**, 445 (1981).

用鎂(25)磁場共振方法來觀察錯離子在水溶液中的結合：DNA-鎂鹽

明尼蘇達大學化學系

梅　宏　綺

摘　要

此篇試驗的系統是 $[MgCl_2]_{init} = 80$ mM 與 $[磷酸根]^{DNA}_{init} = 20$ mM 在高 [NaCl] 濃度與 [NaCl]=0 的情形下來測鎂磁場共振圖的半高長度。試驗結果顯示了鎂鹽-DNA 的靜電相吸的結合領域會被其 supporting electrolyte 的濃度影響。

^{25}Mg NMR THE MAGNESIUM-ATP INTERACTION
— A Multinuclear NMR Study —

ELIZABETH H. MEI*

Department of Chemistry,
University of Minnesota

ABSTRACT

Magnesium-25 NMR line widths are reported for aqueous solutions of adenosine 5′-triphosphate in the pH range from 7–8 as a function of reciprocal temperature for various ionic compositions of the solution. The results indicate that the kinetic and thermodynamic aspects of the magnesium-ATP interaction may be complicated by additional equilibria involving excess ion participation.

INTRODUCTION

The binding of alkaline earth ions to ATP and other nucleotides is critical to the activation, binding, and ultimate function of these molecules in controlling enzymatic activity and therefore a variety of critical processes. Previous work on the solution chemistry of ATP and related molecules is extensive,[1] yet several aspects of such solutions remain incompletely understood, and in some cases controversial.[2] The magnesium-25 NMR spectrum provides a little used method for investigating these metal complexes, and new high field NMR spectrometers largely eliminate the limitations of signal to noise that have previously restricted applications at physiological concentrations. Earlier work on magnesium-25 NMR in ATP solutions has pointed out the importance of the chemical exchange kinetics between the ATP complex and the free ion environment in the solution as possibly controlling the relaxation behavior of the magnesium-25 NMR signal. In the earliest work[3] the temperature dependence of the magnesium-25 line width was interpreted using standard approaches. That analysis required a significant chemical

* Current address: Elizabeth H. Mei, Ph. D., 842 Morningside Drive, Millbrae, CA 94030, U. S. A. Dr. Mei is an alumus of Fu Jen Catholic University.

shift of the magnesium-25 resonance on binding to the ATP. However, at that time, it was not possible to measure the chemical shift accurately as in those solutions the shift was on the order of the line width. However, with present spectrometers the shift may be amplified at least 5- or 6-fold, and this interpretation has been criticized because the large shifts predicted by the earlier analysis are not consistent with the higher field NMR results now available.[4] For this reason we have reinvestigated the magnesium-25 NMR spectrum as a function of concentration, sample composition, and temperature in nucleotide solutions. We have found that the temperature dependence of the magnesium-25 NMR spectrum in adenosine nucleotide solutions is complicated by several factors including what is apparently a metal ion driven aggregation of the nucleotides that depends on both the magnesium and alkali metal ion concentrations in the sample.

EXPERIMENTAL

Disodium ATP was obtained as the equine muscle extract from Sigma Chemical Company. Magnesium-25 was obtained from Union Carbide at Oak Ridge National Laboratories, Oak Ridge, Tennessee. The oxide was dissolved in hydrochloric acid (J.T. Baker Company, Ultrex grade) and evaporated under vacuum to eliminate excess water and hydrochloric acid. The product was dissolved in water and the concentration determined by EDTA titration using Eriochrome black T as an indicator.[5]

The ATP solutions were cleaned of sodium ion by passage through a Dowex-50W-x8 column (Sigma) and the resulting solution titrated to the desired pH with tetrabutylammonium hydroxide (Eastman Chemical Company). The concentrations of the ATP were determined by optical density measured on a Cary 17D spetrophotometer.[5]

The NMR measurements were taken on a Nicolet NT-300 NMR spectrometer using the low frequency broad band probe in an Oxford wide bore magnet. The magnesium resonance frequency in this field is 18.36 MHz. Samples were contained in 12 mm Wilmad sam-

ple tubes and the line widths reported represent the full widths measured at half maximum height of the absorption mode signal.

RESULTS AND DISCUSSION

The temperature dependence of the magnesium-25 NMR line width is shown as a function of reciprocal temperature in Fig. 1 for two solutions of ATP both containing excess magnesium ion. The bottom curve was originally reported by Bryant[5] and obtained at 3.65 MHz while the top curve was obtained at 18.34 MHz where any

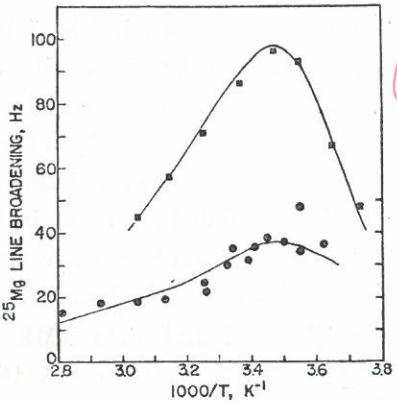

Fig. 1. The dependence of the magnesium-25 NMR line width on reciprocal temperature for solutions containing an excess of magensium ion. (■) Data obtained at 18.36 MHz for a solution containg 0.055 M ATP and 0.747 M $MgCl_2$ at pH 7.7. The solid curve was calculated using an ATP bound line width of 306 Hz, an activation energy for exchange of 15 kcal/mole, and the activation energy for the temperature dependence of the bound line width of 5 kcal/mole. (●) Data reported in reference 3 obtained at 3.675 MHz for solutions containing 1.9×10^{-2} M ATP and 1.5 M $MgCl_2$ at pH 7.9. The solid curve was calculated using an exchange activation energy of 11 kcal/mole and an activation energy for the bound line width of 4 kcal/mole.

contributions from chemical shifts on binding should be five times larger. Since the chemical shift on binding enters the relaxation equation as the square, the earlier analysis predicts that the top curve should be far off scale, which is clearly not observed. In fact, the measurements on equimolar solutions of magnesium ion and ATP indicate that the chemical shifts of the magnesium ion on binding to ATP are actually very small, and certainly smaller than the bound line widths in the present experiments. The error in the earlier analysis that led to the assumption of a considerable chemical shift on magnesium ion binding to ATP appears to be in the neglect of the temperature dependence of the ATP bound magnesium ion line width. The sold curves shown in Fig. 1 include this contribution and a reasonable fit to the data is possibl when the chemical shift on binding is set to zero. However, we note that while inclusion of this dependence provides a reasonable fit to the experimental data, there is reason to believe that such a simple analysis is incomplete because of competing equilibria present in the solutions. We therefore attach no fundamental significance to the parameters used in the calculation of the solid curves in Fig. 1.

The improved sensitivity of high field NMR spectrometrs now permits direct observation of the magnesium NMR spectrum of the magnesium NMR spectrum of the magnesium-um-ATP complex. As part of a careful approach to the characterization of the magnesium-25 NMR in adenosine nucleotide phosphate solutions, we find that the magnesium-ATP interaction may be influenced to a significant extent, as reported by the magnesium NMR spectrum at least, by the addition of monovalent cations. The temperature dependence of the magnesium-25 line width is shown in Fig. 2 for magnesium-ATP solutions. Several features are interesting: (1) Though the magnesium-25 line widths are large by high resolution standards, they are readily measureable, and support the estimates of the bound line widths obtained from application of the rapid exchange models to data taken at excess concentrations of magnesium ion. (2) The temperature dependence of the magnesium-25 NMR line width in Mg_2 ATP complexes is complex and a rather sensitive function of

the ionic composition of the solution. The data shown represent the solutions made in three different ways: (A) with no sodium ion present but with a high concentration of tetrabutylammonium chloride as a supporting electrolyte; (B) with no sodium present, but a low concentration of supporting electrolyte that arises just from the adjustment of pH with tetrabutylammonium hydroxide, and (C) with no supporting electrolyte present, the sodium concentration determined by the fact that the ATP used was the disodium salt and the pH was adjusted with sodium hydroxide, and 3 equivalents of magnesium ion present.

One might argue that the differences between curves A and B of Fig. 2 are due to the changes in both the binding constants and exchange rates that attend the significant change in the total ionic strength in the solution. However, such an explanation is much less

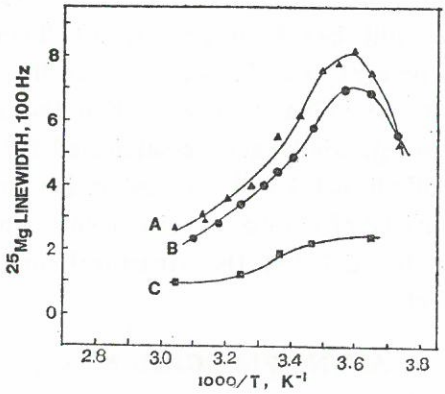

Fig. 2. The magnesium-25 NMR line width as a function of reciprocal temperature for three solutions containing 2 moles of magnesium ion per mole of ATP. (A) Mg_2 ATP concentration at 0.10 M, pH 7.18, with no sodium ion present and a 1.04 M supporting concentration of tetraethylammonium chloride. (B) Mg_2 ATP concentration at 0.10 M, pH 7.18 with the counter ion requirements supplied by tetraethylammonium chloride as described in the experimental section. (C) Magnesium ion and ATP concentrations 0.15 M and 0.05 M, respectively, pH=7.18.

likely for the comparison of curves A and C. An excess of magnesium ion should decrease the magnesium-25 line broadening observed through the chemical exchange mixing of the relaxation parameters for the free and bound magnesium ion environments. However, other things being equal, this mixing should lead to a factor of one-third decrease in the observed line widths. Inspection of Fig. 2 shows that considerably greater effects are observed. Though the magnesium and ATP concentrations used in the present experiments are relatively high, the dramatic effects of excess sodium and magnesium ion on the magnesium NMR spectrum suggests the involvement of these metal ions with ATP in an equilibrium that affects the equilibrium constant or the rate constants that characterize the magnesium-ATP interaction. Metal ion nucleotide interactions have been reported to be important in other nucleotide solutions based on the concentration dependence of the proton NMR shifts where the formation of alkali metal ion mediated structures of several nucleotide molecules per unit has been proposed.[7] Though there is no evidence that the present cases is even structurally similar, we take the present data as preliminary evidence that the magnesium-ATP solutions may be substantially more complicated than has been supposed. Since the alkali metal and magnesium ion concentrations are significant in a variety of cellular environments, further investigation is important for defining the structural and thermodynamic basis of these effects.

ACKNOWLEDGEMENTS

I would like to thank University of Minnesota, Chemistry Department for the use of NMR spectrometer and the support from National Institutes of Health, GM-25757. Thanks also to Prof. R.G. Bryant who initiated this project.

REFERENCES

(1) H, Sigel, Ed., *Metal Ions in Biological Systems*, Marcel Dekker Inc., 1974, Vol. 1, Chap 2.

(2) S.B. Petersen, J.J. Led, E.R. Johnston, D.M. Grant, *J. Am. Chem. Soc.* **104**, 5007 (1982).

(3) R.G. Bryant, *J. Magn. Reson.* **6**, 159 (1972).
(4) S. Forsén and B. Lindman, *Methods of Biochemical Analysis* **27**, 289 (1981).
(5) D.A. Skoog and D.M. West, *Fundamentals of Analytical Chemistry*, Rinehart & Winston. (1974). p. 277.
(6) ε for ATP
$a_M = 15.4 \times 10^3$ at pH=7
P.L. Biochemicals, Inc. Ultraviolet Absorption Spectra p. 2-4.
(7) (i) Same as ref. 2.
(ii) T.J. Pinnavaia, H.T. Miles, E.D. Becker, *J. Am. Chem. Soc.* **97**, 7198 (1975).
(iii) C. Detellier, P. Laszlo, *J. Am. Chem. Soc.* **102**, 1135 (1980).

用鎂(25)磁場共振方法來觀察錯離子在水溶液中的結合：ATP-鎂鹽

梅　宏　綺

明尼蘇達大學化學系

摘　要

此篇報導鎂(25)磁場共振圖（半高長度與溫度倒數）的結果，試驗系統是ATP-鎂鹽的錯離子在 pH=7-8 的水溶液中進行的，而試驗結果顯示 ATP-鎂鹽的結合由 kinetic 及熱力學的觀點來看，反應平衡絕非 ATP+鎂→ATP-鎂一式能描寫的，定有包含其他方式的結合。

比較兩常用聚合物分子量分散率之測定

化學系

陳天鐸　陳壽椿

摘　要

在實驗室裏用 GPC 來測定聚合物之分子量及其分散率是相當平常的一件事，但是，還是需要一些基本的數據才能計算，譬如，需要已知標準分子量之聚合物作參考以及Q因子，如果是使馬克—侯文克之關係式就需要K及α值。不幸的是，前者之準確性不高，而後者在文獻上又缺乏足够的數據資料可供計算。

更重要的是，對羣轉移聚合反應，一種新的聚合反應能產生分子量分佈較窄之聚合物，有興趣的化學家常苦於不知分散率計算方法之準確性及精確性。

本方法是將麻哈巴地(MAHABADI)之計算模式中之控制理論部份以最小平方法取代，寫成電腦程式，然後用標準分子量之聚乙烯苯來作實驗，結果與用傳統的方法作比較。本法不但較精確而且也不需供助於文獻上之K及α值。

前　言

以往在預測聚合體的分子量時，最常用的黏度——分子量關係式爲馬克——侯文克公式 (Mark-Houwink equation)

$$[\eta] = KM^{\alpha} \tag{1}$$

其中M爲非散佈性聚合體的分子量 (monodisperse polymer)。對某一指定的聚合體——溶劑系而言K和α爲常數，通常α介於 0.6～0.8，K介於 0.5×10^{-4} ～ 5×10^{-4} 之間，爲一經驗式。假若所論及聚合體試樣所含分子的分子量大小不一，實驗結果顯示聚合體的本性黏度 $[\eta]$ (intrinsic viscosity) 等於諸非散佈性離份的本性黏度 $[\eta]_i$ 的重量平均，

$$[\eta] = \frac{\Sigma[\eta]_i W_i}{\Sigma W_i} = \Sigma w_i[\eta]_i = K\Sigma w_i M_i^{\alpha} \tag{2}$$

由式(1)，(2)可知其平均分子量 $\overline{M}_v$ 爲

$$\overline{M}_v = \left(\frac{[\eta]}{K}\right)^{1/\alpha} = (\Sigma w_i M_i^{\alpha})^{1/\alpha} \tag{3}$$

雖然由式(3)可求出聚合體的黏平均分子量，但一般都缺乏可靠的馬克——侯文克常數K和α，以致無法得到較正確的實驗結果。

本文引用的方法係參照 H. Kh. MAHABADI 所提之法[1]而加以修改的，

可以直接由分子量分佈和聚合體的本性黏度 [η] 來求出平均分子量 $\bar{M}_v$，並且可以推廣求出合理的馬克——侯文克常數K和 α[2]。

理　　論

首先定義一參數 J 如下[3]：

$$J = [\eta]M = \sum_{i=0}^{n} D_i V_i \qquad (4)$$

其中 [η] 爲聚合體的本性黏度

M爲聚合體的分子量

V爲 GPC 沖提的體積

D爲多項式之係數

由式(3)和式(4)合併可得：

$$\bar{M}_v = (\Sigma w_i J_i^{(\alpha+1)/\alpha})^{(\alpha+1)/\alpha}/[\eta] \qquad (5)$$

再根據馬克——侯文克公式 $[\eta] = K\bar{M}_v^{\alpha}$

取代式(5)中的 $\bar{M}_v$ 可得

$$K = ([\eta]/\Sigma w_i J_i^{\alpha/(\alpha+1)})^{\alpha+1} \qquad (6)$$

或 $$\ln K = (\alpha+1)\ln[\eta] - (\alpha+1)\ln \Sigma w_i J_i^{\alpha/(\alpha+1)} \qquad (7)$$

根據式(7)，我們可從待測物（unknown）的本性黏度和 GPC 圖譜，經由電腦的計算，畫出圖 1 的結果。

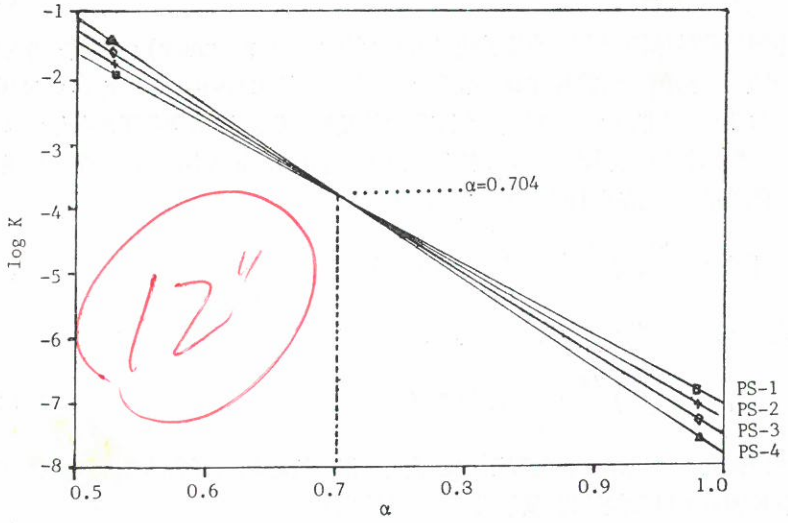

圖 1. log K 對 α 作圖　PS-1: 50K, PS-2: 100K, PS-3: 233K, PS-4: 600K

如此可得 $\ln K$ 和 α 之關係式：

$$\ln K = C - B\alpha \tag{8}$$

許多研究報告[4-6]，均由此一關係式來預測K和α的值。由圖1可知式(8)中的B和聚合體的分子量有關，分子量愈大，斜率B愈大。而從另一方面而言，式(7)對α微分，亦可得到斜率 $-B$

$$-B=\frac{d\ln K}{d\alpha}=[\eta]\ln\sum w_i J_i^{\alpha/(\alpha+1)}-\frac{1}{\alpha+1}\frac{\sum w_i J_i^{\alpha/(\alpha+1)}\ln J_i}{\sum w_i J_i^{\alpha/(\alpha+1)}} \tag{9}$$

從式(5)取代式(9)的 $[\eta]$ 可得：

$$B = \ln \bar{M}_v - U \tag{10}$$

其中

$$U=\frac{1}{\alpha}\ln\sum w_i J_i^{\alpha/(\alpha+1)}-\frac{1}{\alpha+1}\frac{\sum w_i J_i^{\alpha/(\alpha+1)}\ln J_i}{\sum w_i J_i^{\alpha/(\alpha+1)}} \tag{11}$$

如此可明顯地看出B和 $\bar{M}_v$, U（聚合體的分子量分佈係數）間的關係。表1和表2爲聚合體在不同的α時，所求的U值。可以看得出U對α不十分靈敏，即α改變而U的變化却不大；$dU/d\alpha \simeq 0$.

表1. α從 0.5～1.0 之U值（U爲α的函數）

α	$M_v=50,000$ $M_w/M_n=1.04$	$M_v=100,000$ $M_w/M_n=1.05$	$M_v=233,000$ $M_w/M_n=1.06$	$M_v=600,000$ $M_w/M_n=1.10$
0.50	−0.0510	−0.0780	−0.0300	−0.0430
0.55	−0.0521	−0.0783	−0.0310	−0.0432
0.60	−0.0513	−0.0785	−0.0309	−0.0431
0.65	−0.0523	−0.0784	−0.0312	−0.0429
0.70	−0.0526	−0.0793	−0.0316	−0.0431
0.75	−0.0527	−0.0797	−0.0314	−0.4280
0.80	−0.0529	−0.0804	−0.0320	−0.0440
0.85	−0.0531	−0.0806	−0.0318	−0.0443
0.90	−0.0527	−0.0810	−0.0319	−0.0450
0.95	−0.0531	−0.0809	−0.0321	−0.0447
1.00	−0.0532	−0.0810	−0.0320	−0.0450

表2. PS 的 $U_{\alpha=0.5}$ 和 $U_{\alpha=1.0}$

Polymer	M	M_w/M_n	$U\alpha=0.5$	$U\alpha=1.0$
PS-1	50,000	1.04	− 0.051	− 0.053
PS-2	100,000	1.05	− 0.078	− 0.081
PS-3	233,000	1.06	− 0.030	− 0.032
PS-4	600,000	1.10	− 0.043	− 0.045

表 2-1. 不同 α 時的 K 值

α	$M_v=50,000$ $M_w/M_n=1.04$	$M_v=100,000$ $M_w/M_n=1.05$	$M_v=233,000$ $M_w/M_n=1.06$	$M_v=600,000$ $M_w/M_n=1.10$
0.50	2.7366E-02	3.8464E-02	5.6341E-02	8.9828E-02
0.55	7.8075E-03	1.0095E-02	1.3467E-02	1.9151E-02
0.60	2.2275E-03	2.6496E-03	3.2188E-03	4.0830E-03
0.65	6.3550E-04	6.9543E-04	7.6937E-04	8.7048E-04
0.70	1.8131E-04	1.8252E-04	1.8389E-04	1.8558E-04
0.75	5.1728E-05	4.7906E-05	4.3955E-05	3.9566E-05
0.80	1.4758E-05	1.2573E-05	1.0506E-05	8.4354E-06
0.85	4.2105E-06	3.3000E-06	2.5112E-06	1.7984E-06
0.90	1.2012E-06	8.6614E-07	6.0022E-07	3.8342E-07
0.95	3.4272E-07	2.2733E-07	1.4347E-07	8.1744E-08
1.00	9.7778E-08	5.9665E-08	3.4291E-08	1.7428E-08

表 2-2. 不同 α 時的 log K 值

α	$M_v=50,000$ $M_w/M_n=1.04$	$M_v=100,000$ $M_w/M_n=1.05$	$M_v=233,000$ $M_w/M_n=1.06$	$M_v=600,000$ $M_w/M_n=1.10$
0.50	−1.56279	−1.41495	−1.24917	−1.04659
0.55	−2.10749	−1.99588	−1.87074	−1.71781
0.60	−2.65219	−2.57682	−2.49230	−2.38902
0.65	−3.19688	−3.15775	−3.11387	−3.06024
0.70	−3.74158	−3.73868	−3.73543	−3.73146
0.75	−4.28628	−4.31961	−4.35700	−4.40268
0.80	−4.83097	−4.90055	−4.97856	−5.07389
0.85	−5.37567	−5.48148	−5.60012	−5.47511
0.90	−5.92037	−6.06241	−6.22169	−6.41633
0.95	−6.46506	−6.64335	−6.84325	−7.08755
1.00	−7.00976	−7.22428	−7.46482	−7.75876

因此可得：

$$\bar{M}_v = \exp[B(1+\bar{U}/B)] \tag{12}$$

其中 $\bar{U}$ 爲 U 的平均值：

$$\bar{U} = \frac{1}{2}(U_{\alpha=0.5} + U_{\alpha=1.0}) \tag{13}$$

故從式(7)，(11)和(12)即可求出平均黏度分子量 $\bar{M}_v$。

實 驗

藥品：Dupont PS standards (分子量 4K, 9K, 50K, 100K, 233K, 390K, 600K, 1,800K) 以 THF 爲 GPC 溶洗液。

儀器：

1. 日製 Shimadzu Liquid Chromatography LC-3A 接 Spectrophotometric Detector SPD-1
2. 注射器：Hamilton Syringe 50 μl
3. 8 位元電腦：CPU 6502, 192K RAM
   16頻道12位元類比/數值轉換器
   Appligration II 色層分析資料處理套裝軟體
4. 16位元電腦：CPU 8088, 640K RAM
   Lotus 1-2-3 套裝軟體，作爲資料處理

步驟：

以 THF 稀釋成之 PS 標準溶液 (M=4K, 9K, 50K, 100K, 233K, 390K, 600K, 1,800K) 打入 GPC 後，由紫外光檢出器傳出信號透過 A/D 轉換器直接與上述電腦連線，然後由 Appligration II 軟體處理基本資料，再根據上述公式寫成培基 (BASIC) 程式計算結果。最後再以 Lotus 1-2-3 整理出實驗結果列表得之。待測之樣本以購得之 PS 標準如 M_w=4K, 9K, 3.9×10^5, 1.8×10^6 打入 GPC 中。

結果與討論

根據本文所提之方法和傳統 K, α 之方法，結果比較列於表 3，我們可以看出兩種方法所求得之分量十分接近，且由表 4 和表 5 可以發現本法在求K和α之

表 3. 計算的黏度平均分子量 M_v2 (本法)

Sample	M_w/M_n	M_v2	M_v1	M	M_v2 (%)	M_v1 (%)
PS	1.09	3,650	3,647	4,000	−8.75%	−8.83%
PS	1.06	9,366	9,359	9,000	4.07%	3.99%
PS	1.04	51,120	51,090	50,000	2.24%	2.18%
PS	1.05	102,658	102,578	100,000	2.66%	2.58%
PS	1.06	242,870	242,740	233,000	4.24%	4.18%
PS	1.10	393,978	392,824	390,000	1.02%	0.72%
PS	1.11	647,160	646,650	600,000	7.86%	7.78%
PS	1.10	1,838,416	1,837,335	1,800,000	2.13%	2.07%

M_v1 用 K=0.000162, α=0.706 計算的分子量

表4. 不同 PS 之 ln (M_v2) 和 ln (Visc.)

Sample	M_v2	Viscosity	ln (M_v2)	ln (Visc.)
PS	3,650	0.0566	8.2025	−2.8723
PS	9,366	0.1003	9.1448	−2.2998
PS	51,120	0.3365	10.8419	−1.0892
PS	102,658	0.5489	11.5392	−0.5998
PS	242,870	0.9974	12.4003	−0.0026
PS	393,978	1.4349	12.8841	0.3611
PS	647,160	1.9449	13.3803	0.6652
PS	1,838,416	4.2241	14.4244	1.4408

表5. 馬克——侯文克常數

Sample	Solvent	K	α	Remark
PS	THF	0.000162	0.7060	1
		0.000179	0.6963	2
		0.000164	0.7040	3

1. 參考值
2. ln [η] 對 ln [M_v2] 計算斜率和截距
3. 本法中，圖1的任何兩直線交點所求之K和 α

結果，令人十分滿意。在文獻上，許多聚合體尚缺乏K與 α 值，尤其是新合成之聚合體更是如此，如果應用本文所述之方法可以很容易求出K和 α 值。

以表6列出兩種方法之間的差異。

表6.

	本　　法	傳 統 方 法
Standards	少　　數	多　　個[7]
K, α	不　　用	缺 乏 資 料
Mv	± 8 %	± 8 %
[η]	實 驗 求 得	由 K, α 計算可得

〈i〉 J 的求法

根據 MAHABADI[1,7,8] 所提 J 之求法比較複雜，本文則使用較簡便的方

法，可減少找參數Q的時間和誤差，但却須至少三個 standards 才可靠。方法如下：

根據J的定義

$$J = [\eta] M = D_0 + D_1 V + D_2 V^2 + \ldots \tag{14}$$

對J取自然對數得

$$\ln [J] = \ln [D_0] + \ln [D_1] + \ln [V] + \ln [D_2] + 2 \ln [V] \tag{15}$$

則 $\ln [J] = A + M \ln [V]$ 爲一直線，再利用最小平方法（L.S.）可以把 A, M 找出，如此亦可得到 $J = \exp [A + M \ln [V]$ 之關係，不過此時經過 L.S. 之後，會產生少許的誤差，所幸經本實驗之結果表3，發現誤差還不算太大，但却需要先利用 standards 來建立J函數，有別於 MAHABADI 所提之法，不須用 standard 即可找出J函數。

〈ii〉 **B 的求法**

根據式(9)和式(10)，我們以 $\alpha = 0.5 \sim 1$ 求出相對應之 ln K 如表2所示，再經 L.S. 求出斜率即可。

〈iii〉 **U 的求法**

在理論部分得知U幾乎爲一常數，不受α的影響，而只和分子量大小有關，如表1和表2，因此可用 $\alpha = 0.5$ 和 $\alpha = 1.0$ 代入求出 $U_{\alpha=0.5}$ 和 $U_{\alpha=1.0}$，然後再取平均 $\bar{U}$，如式(13)所示。

〈iv〉 **K 和 α 的求法**

方法一：

根據式(1)，$[\eta] = K M_v^{\alpha}$，取自然對數得

$$\ln [\eta] = \ln K + \alpha \ln [M_v] \tag{16}$$

然後以 $\ln [\eta]$ 對 $\ln [M_v]$ 作圖，即可得K和α。

如圖2和表4。

方法二：

以 ln K 對 α 作圖，如圖1，我們知不同分子量有不同的直線 $\ln K = C - B\alpha$，所以任何二條直線之交點即可得到K和α。

由表5，比較方法一和方法二的求法，發現方法二所得之結果較接近標準值。

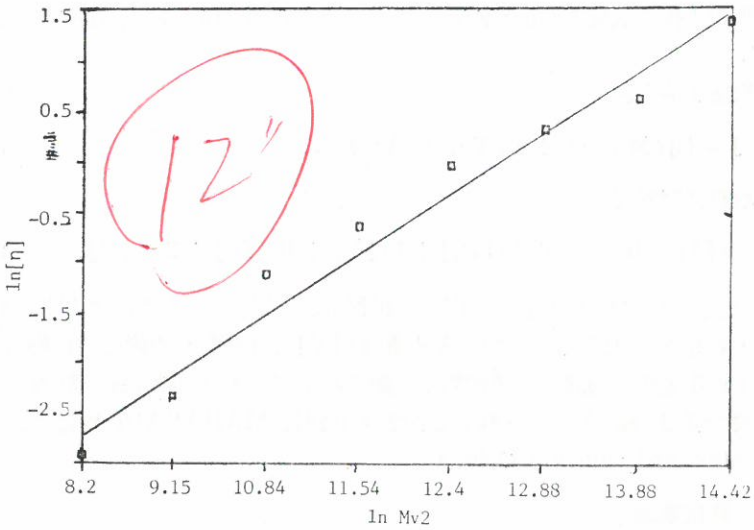

圖 2. ln[η] 對 ln Mv2 作圖
斜率：0.6963　截距：−8.6279

結　語

以往只能靠馬克——侯文克公式來求得聚合體之分子量，而且文獻上，K與 α 值的缺乏更是一大困擾。本文所提之方法，不但不需要常數K和 α，反而可以由已知條件及公式推求出K和 α。當然最重要的還是此法的準確性非常高。

誌　謝

此次研究報告十分地感謝聖言會資助部份電腦設備，並感謝吳英郎學長在百忙中的鼎力相助，以及周善行教授和牛昭文學長所提供的 GPC 資料，深感銘謝。

參考文獻

(1) H. Kh. Mahabadi, *J. Polym. Sci.* 22, 449 (1984).
(2) F. W. Billmeyer, *Experiments in Polymer Science, Interscience* (John Wiley & Sons, New York, 1973).
(3) J. N. Cardenas and K. F. O. Driscoll, *J. Polym. Lett. Ed.* 13, 13, 167 (1975).
(4) M. Szesztay and F. Tudos, *Polym. Bull.* 5, 429 (1981).
(5) S. M. Aharoni, *J. Appl. Polym. Sci.* 21, 1323 (1977).
(6) K. Kamide, A. Kataoka, A. L. Resnik and R. J. Samuels, *J. Polym. Sci.* 17, 391 (1955).

(7) W. W. Yan and C. P. Malone, *J. Polym. Sci. Lett.* ed. 5, 663 (1967).
(8) W. W. Yan, M. E. Jones, C. R. Ginnard and D. D. Bly, *Am. Chem. Soc. Symp. Ser.* 138, 91 (1980).

Comparison of Two Popular Universal Calibration Methods for Polydispersity Determination by Gel Permeation Chromatography

TAIN-DOW CHEN and SHOW-CHUEN CHEN

Department of Chemistry

ABSTRACT

Although the determination of polymeric molecular weights and polydispersity by GPC is by no means a formidable task, it does demand some minimum number of parameters to be known, for example, it requires polymer standards and Q factor or, K and α values if Mark-Houwink relationship to be implemented. Unfortunately, the former, the Q-factor method, falls short of accuracy and the latter, Mark-Houwink relationship, is handicapped because the literature lacks sufficient data for calculation.

More importantly, the chemist interested in Group Transfer Polymerization, a new process capable of producing narrow-range-molecular-weight polymers, needs to know the accuracy and the ability to differentiate the polydispersities of the method for determination that he employes. The present method, modified for simplicity by substituting the least suare for the control theory from Mahabadi's model, was implemented with polystyrenee standards on an on-line 8-bit Apple II Microcomputer and was compared to the conventional method. It offers the advantages of accuracy and self-sufficiency without the use of documented K and α values.

銅及銀離子選擇電極之改進

化學系

饒忠儒　李榮忠　陳壽椿

摘　要

以碳爲基材之固態離子選擇電極不但易作而且靈敏度高。但是在某些干擾離子之存在下，電極會受到不可逆之損害。尤有甚者，如果電極保存不當還會有線性範圍變窄，感應遲鈍及斜率降低的現象。

上述之種種問題都可以改用 1M 的浸泡溶液及表面處理的方式來改良。

I 引　言

介紹銅離子與銀離子選擇電極測定之原理，可見於一般的文獻上[1]。其一般的表示法爲：

$$E_{cell} = E_{ind} - E_{ref} + E_j$$

其中：E_{ind} 爲 indicator electrode potential

E_{ref} 爲 reference electrode potential

E_j 爲 junction potential

由於 E_{ref} 一般而言，均爲一常數，而 E_j 又可予以忽略，根據能斯特 (Nernst) 公式，我們可以得到：

$$E_{cell} = E_{const} + \frac{RT}{nF} \ln a_j$$

a_j 爲待測離子之活性

在一般情況下，$E_j = 0$，則 $E_{const} \doteqdot E_{ref}$，如欲詳細討論，則可得到以下的方程式[2]：

$$E_{cell} = E_j + E_M - E_{ref}$$

其中：E_M 爲 Membrane Potential，又

$$E_M = E_D + E_B$$

其中：E_D 爲 Diffusion Potential

E_B 爲 Boundary Potential

II 實　驗

一、試劑及器材：

碳棒（拆自 3 號電極）

氯化鉀（Merck）
硫酸銅（Merck）
濃鹽酸（Merck）
硫化鈉（Merck）
硝酸銀（Merck）
纖維醋酸酯（Cellulose Acetate: 和光純藥工業株式會社）
丙酮（Merck）
PVC 管
鋁箔
喇叭線（同軸雙心線）
二液型環氧樹脂（市售 AB 膠）
快乾膠（Cyanoacrylate Adhesive）
脫離子水（17 MΩ）

二、儀器：

PH Meter: JENCO 6209
ORION DIGITAL 701
FISHER Accumet Model 220

三、步驟：

電極製備法參照參考文獻[3]

A．硫化銅電極：（電極 C、D）

①將碳棒浸入濃鹽酸中，置入超音波中振盪 5 分鐘，取出，倒掉鹽酸，再添入，再振盪，直到鹽酸中不再有黑色混濁，或沈澱爲止，倒掉鹽酸。
②加入新的濃鹽酸，浸泡碳棒，置於通風櫥中，至少靜置一夜。
③取出碳棒，以清水冲洗後，浸入 1M 的硫酸銅溶液中，靜置一夜。
④取出碳棒（不可清洗）直接浸入 1M 的硫化鈉溶液中至少 4 小時。
⑤取出碳棒，陰乾後，以拭鏡紙輕輕磨光碳棒表面約 5 分鐘。
⑥將碳棒套入 PVC 管，以二液型環氧樹脂合口（約 6 小時）。
⑦將飽和的氯化鉀溶液灌入 PVC 管中，至半滿，做爲內導液。
⑧置入由導線，以鋁箔封口，以快乾膠爲接着劑，製造時應避免導線內之金屬線與鋁箔接觸，以免產生干擾。
⑨配製 10^{-1}～10^{-7}M 的硫酸銅標準溶液，並測各濃度的E值，作校正曲線。
⑩求線性範圍，斜率，以及 γ 值（相關係數）

B．硫化銀電極：（電極 A、B）

①將 1M 的硫酸銅溶液換爲 1M 的硝酸銀溶液，重覆A之①～⑩步驟。

②取任一位於校正曲線線性範圍內之濃度，測其電位值，每10秒鐘讀值一次，連續30分鐘，以電位對時間作圖，求出感應曲線(Response Curve)。

C．纖維醋酸酯薄層的塗佈法[4]：(電極E、F)

①取出經由A步驟所完成的電極，浸入纖維醋酸酯5%的丙酮水溶液中4～5分鐘。

②緩緩將電極垂直由溶液中提出，在冷藏庫乾燥約15分鐘。

③由冷藏庫中將電極取出，浸於冰水中1小時。

④電極先將碳棒裹蠟，以砂紙及無纖維紙依序先後磨光兩端，再做C之①～③步驟。

Ⅲ 結果與討論

電極浸泡溶液之濃度

在製備電池的過程中，所有的溶液均用1M而不用飽和溶液，其原因是，在碳棒浸過飽和溶液後，在碳棒上會殘留該溶液的結晶，由於在浸泡過程中，碳棒不能以水清洗，故此類晶體的存在，徒增處理上的困難，改用1M的溶液後，基本上，溶液仍屬於高濃度之溶液，而不會有殘留的晶體在碳棒上，處理方面較爲容易。

校正曲線（Calibration Curve）的不連續性

在製備電極時，我們發現，如果碳棒上只有塗佈上一層時，其感應（Response）最快，但大部份的電極會不大穩定，即由線性廻歸求出的γ值不理想，約0.85，此時，如再塗佈上一層，一般而言，可以得到較理想的結果，然而，當塗佈達二層以上時，線性範圍雖會增加，但是，校正曲線有時會產生如圖1之不連續現象。其中的二段直線，互爲平行線此時，重覆實驗步驟A之③～⑤，再塗佈上一層硫化銅（或硫化銀），或者浸泡在水中達一小時以上，均可使此情況消除，惟此種現象生成的原因，目前仍不完全明瞭。

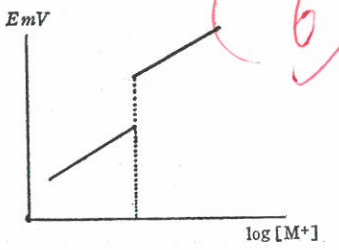

圖 1.

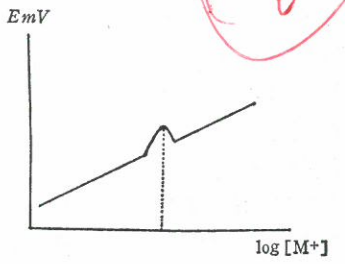

圖 2.

電極之保存

電極如果保存在某一固定溶液中（例如硫化銅電極浸在濃度爲 a_0 的銅離子水溶液中）達一小時以上，取出後馬上測其電位，則其校正曲線會有二種情形，一是如圖1的情形，其中二線段不連續點所對應的濃度，即爲該保存溶液之濃度（a_0）。而第二種情形，則是校正曲線在保存溶液的濃度時，其 E_{mv}（電位）值有特別高的現象，如圖2所示，而此二種問題可以藉浸泡於水中一段時間來解決。

碳電極使用上的限制

由於未保護的碳電極，如電極C、D，的穩定性較差，在長期浸泡於水中達一星期時，線性關係即消失，而每日所測得之校正曲線，斜率的變動亦很大，因此在使用時，就遭到了一場限制。由於此類電極在做連續測試時，其連續測試的二濃度的差，不能大於100倍（即 $\Delta PI<2$）。而且在連續兩次做校正曲線時，第二次校正曲線的線性範圍及 r 值均較第一次爲佳。因此，在量度一未知物的濃度時，其正確方法爲，先做一次校正曲線，求出一線性方程式，再測未知物的電位，代入上述方程式中，求出大約的濃度，再將此濃度增減10倍，測三點的電位，求出第二條線性方程式，再測未知物的電位，代入第二個方程式中，未知物的精確濃度即可測出。例如，未知物的濃度爲 3.67×10^{-3}M，那麼在做完校正曲線後，先測一次未知物，而得到其大約濃度爲 10^{-3}M，然後再測 10^{-2}M，10^{-3}M，10^{-4}M 三點的電位，求出第二條線性方程式，此時，再測未知物一次，將所得之電位值代入第二次求出之方程式中，即可解得精確的未知物濃度。

上述的操作方式，的確繁瑣，而此種操作上的不便，可以藉着在電極上再塗佈上一層保護膜而予以解決，而保護膜的作用即是用來降低電極上離子與溶液中離子的交換作用而達保護之效果。初步我們採用纖維醋酸酯作爲保護膜之材料，效果不錯，其妙處將於後文漸次提及。但是它會降低電極的斜率，如圖3及圖4，其斜率較之表2加膜後之電極的斜率，高出甚多。

線性範圍及斜率穩定性之改進

當逐日追踪觀察一支電極的校正曲線時，我們發現斜率有降低的趨勢，由於 E_{mV} 值爲負，故直線的傾斜度愈來愈大，有時這種變化會很大，往往今天測得之斜率爲 -33mV，第二天即跳到 -67mV。而其線性範圍會日漸縮少，E° 值（截距）亦不穩定，其間差值可以高達 100mV 以上，而且當此一電極連續的浸在水中達7天以上，其線性即完全消失，而且無法經任何處理方式使其再生，必須將碳棒重新依實驗步驟再重新製備。但如乾燥保存，則其壽命可以保存得很久，半年以上亦不會衰退，至於斜率的穩定，線性範圍的固定以及在水溶液中保存時限的加長，如果用纖維醋酸酯保護膜保護，均可以得到人人滿意的結果，只有 E° 值（截距）的穩定仍有困難。

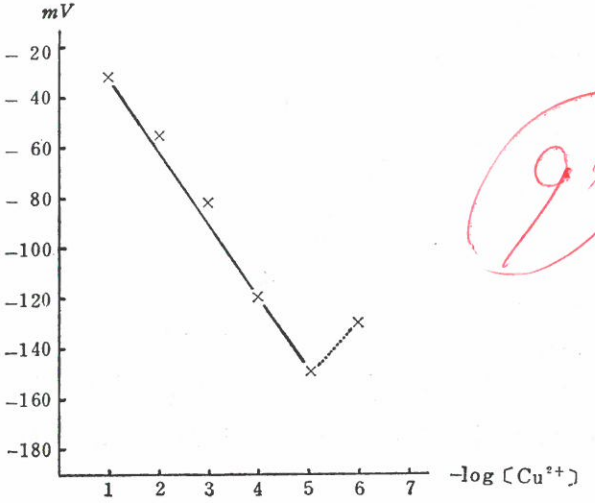

圖 3. 電極C，線性範圍1×10^{-1}～1×10^{-5}，斜率 −30.1，E° 值 −2.5

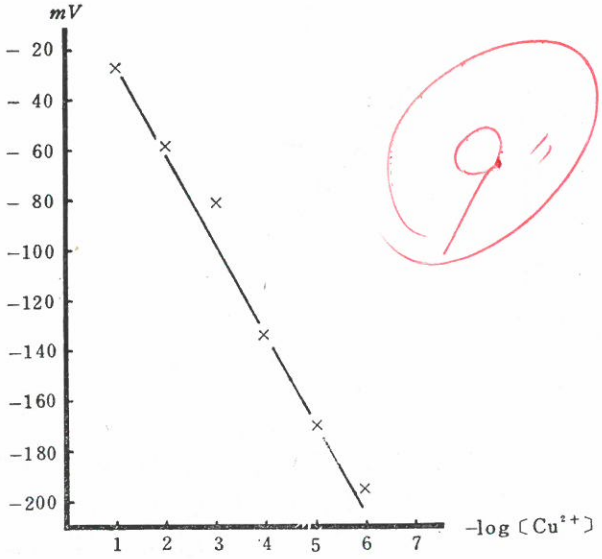

圖 4. 電極D，線性範圍 1×10^{-1}～1×10^{-6}，斜率 −35.2，E° 值 −12.5

其次，在測試電極時，發現間隔10～15分鐘，再作一次測試，其線性範圍及斜率之絕對值有增加的情形，如圖 5 及圖 6 。以上的問題除了使用薄膜保護外，另一項解決的方法是以 10^{-3}M 硫酸銅溶液來浸泡電極，作爲測試的前處理，如

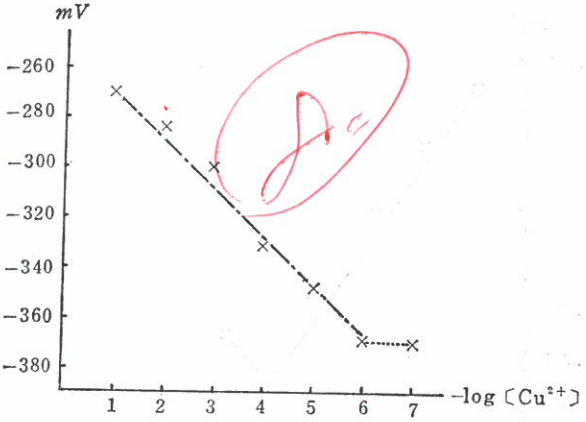

圖 5. 電極 E，線性範圍 1×10^{-1}～1×10^{-6}，斜率 −20.5，E° 值 −245.5

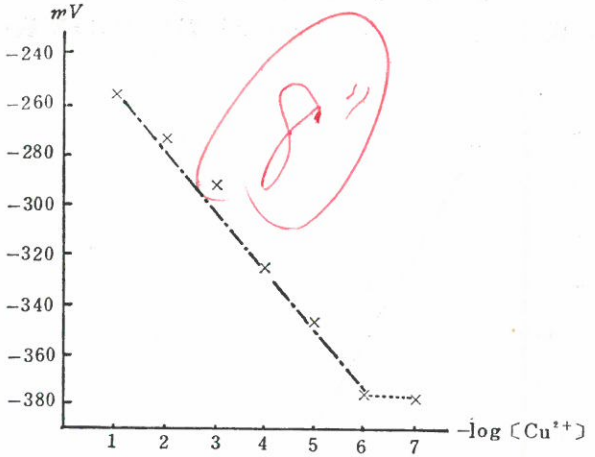

圖 6. 電極 E，線性範圍 1×10^{-1}～1×10^{-6}，斜率 −24.2，E° 值 −226.8

電極 E，所得之結果如圖 7、圖 8、圖 9 及圖10，其線性範圍均未改變，而斜率也相當穩定。但浸泡時間不足30分鐘則並未收到預期的效果，而如果時間超過一小時以上，卽又會出現前面所提及的不連續現象如圖 1 及圖 2，因此，浸泡之時間以30分鐘至一小時之間爲佳。

E° 值的變化

由實驗觀察得知，電極的 E° 值有逐日升高的趨勢，而有一次，電極 E 之封口沒有封死，使由導液 $KCl_{(aq)}$ 蒸發，因此重新填加 $KCl_{(aq)}$，更換導線，發現電極的值有明顯的改變。

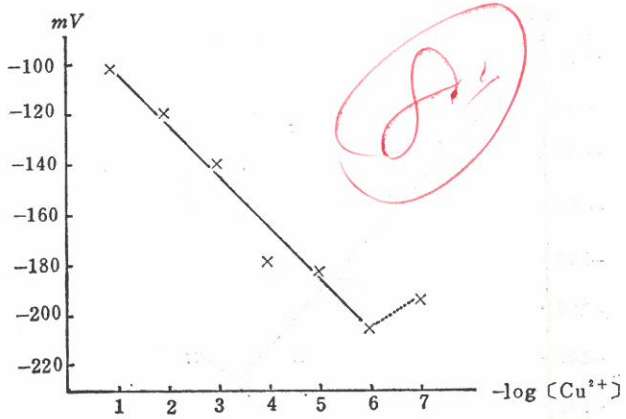

圖 7. 電極E，線性範圍 1×10^{-1}～1×10^{-6}，斜率 −21.8，E° 值 −79.0

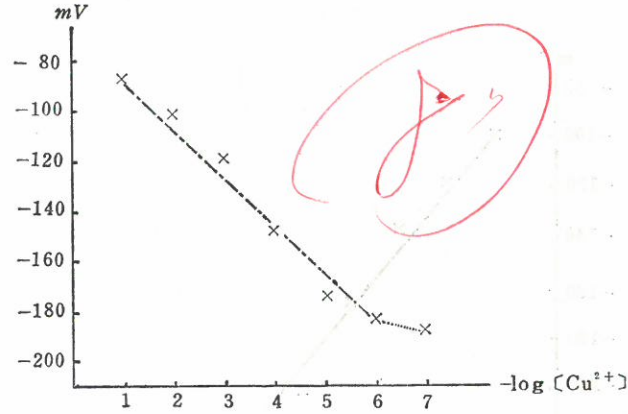

圖 8. 電極E，線性範圍 1×10^{-1}～1×10^{-6}，斜率 −20.9，E° 值 −63.7

電極之儲存

在電極的儲存方面，我們覺得最困難的是發霉的問題，一旦發霉，整支電極就完全喪失作用了，因此，我們建議，如在保存溶液中加入 0.01％的叠氮化鈉（$N_a\ N_3$），便可達防霉的效果，但不可過量，如過量，則溶液中之銅離子均會被其還原成亞銅離子，這可以由溶液之顏色由藍色明顯的轉變爲綠色而得到證明，而且叠氮化鈉的毒性極强，它與酸性物質在一起時，易引起爆炸，應該特別小心。

電極壽命之延長

當我們對一支電極的校正曲線做連續的追踪觀察時發現，當線性範圍開始縮

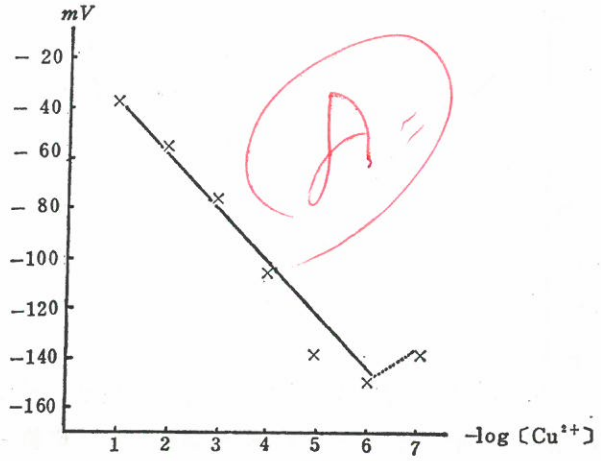

圖 9. 電極E，線性範圍 1×10^{-1}～1×10^{-6}，斜率 −23.7，E° 值 −9.7

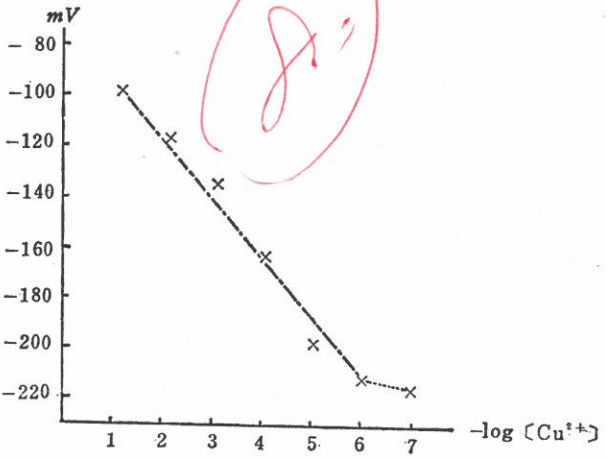

圖10. 電極E，線性範圍 1×10^{-1}～1×10^{-6}，斜率 −24.1，E° 值 −68.5

小時，其方向是由可測得之最高濃度及最低濃度開始向中間縮小，一般而言，當硫化銅電極連續泡在水中 2～3 天後，其線性範圍會由 10^{-1}～10^{-7}M 縮少至 10^{-2}～10^{-5}M，而此一線性範圍可以維持約 3 天，但是如果加上了纖維醋酸酯的薄膜後，線性範圍就可以持續很久，例如電極E在加膜後測其電位，在 8 月 8 日測得其線性範圍爲 10^{-1}～10^{-5}M，到了 8 月28日再測時，其線性範圍仍爲 10^{-1}～10^{-5}M，其間泡在水中整整21天，而線性範圍絲毫未變，比起一般電極 7 天的壽命要長 3 倍以上，薄膜保護的功用由此可見。

硫化銀電極之校正曲線

硫化銀的校正曲線，很明顯的有二段線性範圍（如圖11及圖12），其斜率的正負號正如相反，但以其斜率來看，理論值爲 59.1，故線性範圍應是在 10^{-1}～

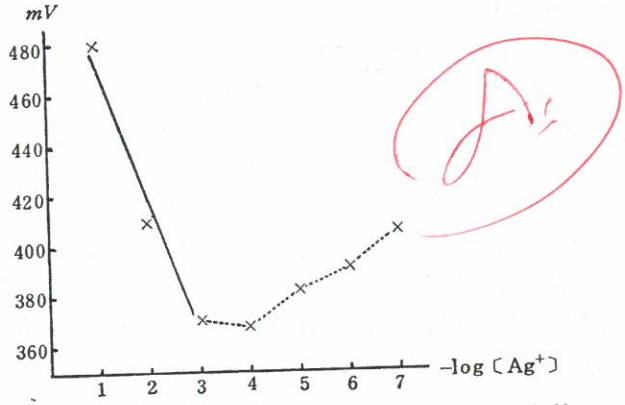

圖11. 電極A，線性範圍 1×10^{-1}～1×10^{-3}，斜率 −55.0，E° 值 530.0

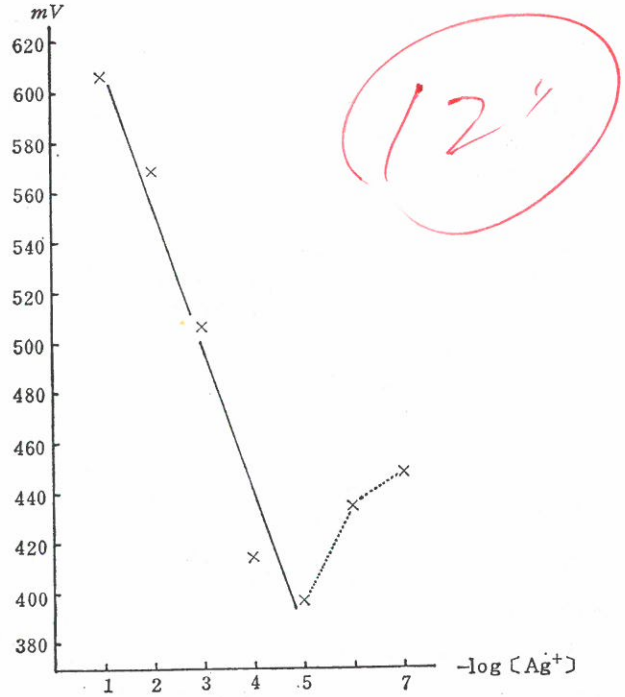

圖12. 電極B，線性範圍 1×10^{-1}～1×10^{-5}，斜率 −57.5，E° 值 670.7

10^{-5}M 之間才對（電極 B 之斜率爲 −57.5），但 γ 值在此一範圍中反而較小，此一缺點，可以由加入硝酸，調整 pH 值近似於 6，使得氫氧化銀（$Ag(OH)_2$）無由生成，銀離子的濃度即可固定，較佳的維性關係即可得到。

校正曲線讀值的時間

在測試電極時，要等電位穩定大概需要 5 分鐘，所需時間太長，實不經濟，若在10秒時即取值，又因時間太短不易控制，所以延長至20秒取值，如表 1，其斜率與以 5 分鐘取值的相差很小，幾乎與之平行，如圖13。由公式所推得之曲線，只要在線性範圍內之濃度，在相同時間內取值也有一定之線性關係。但是，以上所言僅通用於感應良好的電極，如感應不好的電極其間二值會差很多，斜率也不會如上述般的理想，至於電極感應的良好與否，則取決而感應曲線（Response Curve）之圖形，以及感應時間（Response Time）。另外，由實驗中發現，在測試電極時，由低濃度往高濃度測，可得到較好的線性關係，如圖10，但是，由高濃度往低濃度測，其線性關係依然存在。如圖14。

表 1. 電極 E，連續追踪測試，20秒、5 分鐘取值，斜率比較表

日期	（8月份）	8	11	12	14	18	20	22	26	28
斜率	20 秒 取 值	−16.9	−21.7	−19.3	−24.3	−23.4	−21.1	−20.2	−23.1	−22.2
	5 分鐘取值	−16.1	−21.8	−18.8	−23.7	−23.1	−20.1	−20.5	−22.9	−22.7

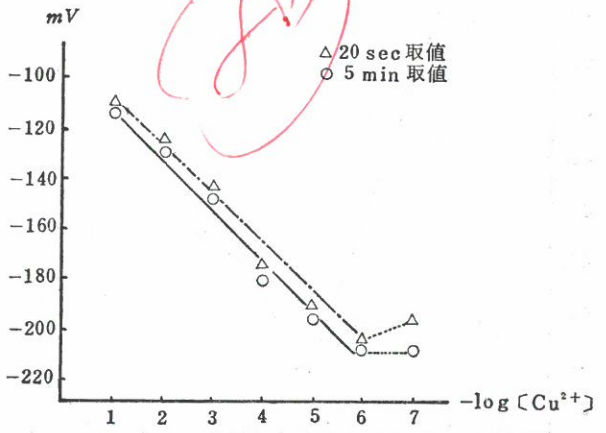

圖13. 電極 E，線性範圍 1×10^{-1}～1×10^{-6}，斜率 $\frac{20\text{ sec 取值}\ 19.6}{5\text{ min 取值}\ -20.2}$，E°值 $\frac{-88.5}{-89.2}$

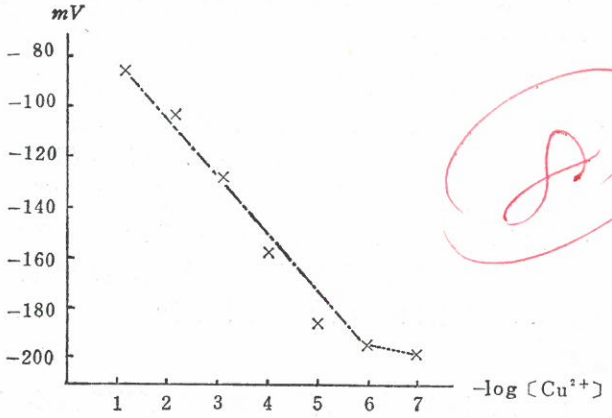

圖14. 電極E，線性範圍 1×10^{-1}～1×10^{-6}，斜率 −23.1，E° 值 −59.5

感應曲線及感應時間

我們在測量電極的感應曲線時發現，在測試感應曲線之前電極所保存的溶液濃度如大於測試的濃度時，我們可以得到如圖15的曲線，如低於測試時的濃度，則可以得到如圖16的結果與文獻上之紀載相符（詳見參考文獻(5)及文獻(6)）。

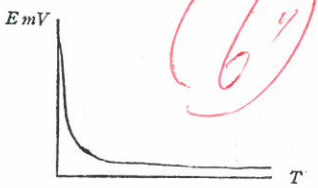

圖15.

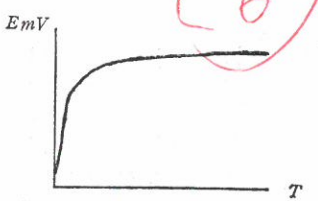

圖16.

至於感應時間（詳見參考文獻(7)）固然是愈短愈好，但曲線平滑的程度亦非常重要，在二者不能兼顧時，我們以爲曲線的平滑程度是較爲重要的考慮因素，如果曲線相當的平滑，則我們在做校正曲線時，如果讀取的時間分別在20秒或5分鐘時，所做出的二條直線幾近於重疊，但是如果感應曲線相當粗糙的話，那二條校正曲線非但不能重合，而其斜率甚至也會相差很大，所得到的 γ 值也較差，由此，我們即可判別電極的穩定程度。如果感應曲線非常的平滑，而感應時間也很短，當然是最好，但是，目前爲止，似乎尚未有如此理想的情況出現。

干擾離子效應

當我們測量電極的K值時發現，如果干擾離子的强度大於一級離子（Prim-

ary ion)，即 ksp 小於一級離子時，在測過K值之後，可能是由於干擾離子與電極上的一級離子發生離子交換作用，而改變電極的表面性質，此時，如再測此電極的校正曲線，就觀察不到線性關係的存在，解決此種困擾，可以浸入10^{-3}M 的 EDTA 溶液中約20分鐘來除去干擾離子（有關 EDTA 的資料請參照參考文獻(8)），再將電極浸入飽和的一級離子溶液中，使電極再生。但是徹底的解決方法，還是利用薄膜層保護法，由利用纖維醋酸酯的結果可知有相當大的改進，它使得在測完K值後，再量度 10^{-3}M 銅離子溶液的電位時，與在測K值前所得之量度值，二者的差在 5 mV 以下，結果可以說不錯。測量K值的方法參照參考文獻(9)～(11)，因爲K值之資料不全，將來會另外發表。

薄膜厚度的選擇

碳棒電極製作完成後，若不加膜保護，則線性範圍很快就縮小，甚至沒有線性。因此，以纖維醋酸酯之丙酮水溶液來製膜，配方係參照逆滲透膜之製法(4)。膜的厚度與其溶液濃度有很大的關係。濃度爲20%之溶液所做成的電極，其感應時間加長。濃度爲2%，3%的溶液，在乾燥時又因濃度稀薄，薄膜一製成即乾裂爲微少的細片。所以選擇以濃度爲5%的溶液來保護電極。

電極加膜前後的比較

表2.

		電極 E	電極 F
加膜前	斜率	−27.6	−22.3
	線性範圍	10^{-1}～10^{-6}	10^{-1}～10^{-6}
加膜後	斜率	−12.5	−22.6
	線性範圍	10^{-1}～10^{-7}	10^{-1}～10^{-6}

如表2可見電極E校正曲線的斜率的絕對值有下降的情形，電極F之斜率差異較小。造成這些差異的原因，可能在於電極E之薄膜厚度不均勻，其下端平面厚度最厚，此係纖維醋酸酯溶液的附着力與由張力的影響。而圓柱表面上之膜，由於是垂直置於冷藏庫中乾燥，因重力的作用，導致上端較薄，下端較厚，電極F僅有下端單一平面沾上膜，其厚度差異很小。

Ⅳ 結　　論

大致上，直接由碳棒製成之離子電極如不加以改進，就會有穩定性差、斜率變動大、線性範圍會隨使用的時間而漸漸縮小，E° 值（截距）也不穩定之缺點，而且電極本身極易受溶液之濃度及干擾離子的影響，而改變其本身的表面性質，

使得電極使用壽命縮短。這些問題可以利用薄膜加層保護，而予以有效的解決，在本文中，我們以纖維醋酸酯來塗佈，發現相當的成功。不論斜率，線性範圍都相當穩定，即在電極的壽命方面，也有令人滿意的結果。一支電極在連續浸在水中21天後，亦不會改變其斜率及線性範圍，這是本實驗室以前的電極所沒有的。但是由於纖維醋酸酯的化性較差，故有使用上的限制，與海水淡化膜一樣，僅能長期的使用在 pH＝4～7 的水溶液中，而且電極的 E° 值仍不能予以固定。至於後一項由實驗得知，不同廠牌的碳棒 E° 值的差別很大，因而推測是材質的關係，因此，在薄膜材料及電極本身材料的選擇，以確實的掌握 E° 值，應是我們以後朝向對離子選擇電極做更深入了解的努力方向。

參考文獻

(1) R.E. Lamb, D.F.S. Natush, J.E. O'Reilly and N. Watkins, *J. Chem. Educ.* 50, 432-434 (1973).
(2) W.E. Morf, *The Principles of Ion-Selective Electrodes and of Membrane Transport* (Elsevier Scientific Publishing Co., Amsterdam, 1981), Chap. 9.
(3) A. Paianlvel and P. Rlyazuddin, *J. Chem. Educ.* 61, 920 (1984).
(4) P.A. Schweitzer Ed., *Handbook of Separation Techniques for Chemical Engineers* (McGraw-Hill, New York, 1979), Part 2, 2.1 Membrane Filtration.
(5) Eron Linder, Klara T'oth and Ernö Pungor, *Anal.* Chem. 48, 1071 (1976).
(6) W.J. Blaedel and D.E. Dinwiddle, *Anal. Chem.* 46, 873 (1974).
(7) Arthur K. Covington, *Ion-Selective Electrode Methodology*, Vol. I, (CRC Press Inc., Roca Ration, Florida, 3rd. Printing, 1984), Chap. 9.
(8) Nj. Radic and M. Vudrag, *J. Electroanal Chem.* 178, 321 (1984).
(9) Charles R. Martin and Henry Freiser, *Anal. Chem.* 57, 512 (1980).
(10) H.J. James, G. Carmack and H. Freiser, *Anal. Chem.* 44, 853 (1972).
(11) K. Srinivasan and G.A. Rechnitz, *Anal. Chem.* 41, 1203 (1969).

The Improvements of Copper Ion and Silver Ion Selective Electrodes

JONG-RU RAU, RONG-JONG LII
and SHOW-CHUEN CHEN

Department of Chemistry

ABSTRACT

Carbon-based Solid-state Ion Selective Electrodes grant simplicity and sensitivity, however, they are prone to irreversible damages by some interferent metal ions and also tend to deteriorate if not stored properly, as evidenced by poor linear range, slow responses and decrease in slope.

Considerable improvements such as the use of 1M solutions instead of saturated solutions for soaking and the surface treatment of the electrodes were made to solve the foregoing problems and to extend the life of the electrodes.

THE FINE STRUCTURE OF THE GILL FILAMENT IN *GOMPHINA VENERIFORMIS* LAMARK

WEN-HUEI T'SUI

Department of Biology

ABSTRACT

Transmission and scanning electron microscopies were used to study the fine structure of the gills of *Gomphina veneriformis* L.

The main part of the gill filament is covered with various groups of ciliated and non-ciliated cells. There are great differences in size, shape, composition and function. Five different groups of cilia and cirri were found on the various regions of the gill filaments.

1. The frontal cilia are the long, nonbranched cilia on the frontal surface of the gill filaments.
2. The pro-latero-frontal cilia are usually short with an expanded disc-shaped end and form a row of cilia along each side of the frontal cilia.
3. The sensory ciliary tufts are longer cilia which are interspersed at irregular intervals among the pro-latero-frontal cilia.
4. The eu-latero-frontal cirri are large and complex. Each cirri is composed of pairs of cilia arranged in two parallel, alternating rows. Individual cilia leave the shaft of the cirrus at regular intervals on each side.
5. The lateral cilia are an ordinary type of cilia which are present on each side of the filaments.

INTRODUCTION

The Bivalvia, *Gomphina veneriformis* Lamark, has a very solid, compressed trigonal shell. They are distributed from central Japan south on the fine sandy bottoms in shallow water. They are important as a food-source in Taiwan, and are even artifically raised on a large scale on the western sea-board of Taiwan. They are filter-feeders with extreme development of the gills. Food is taken with the aid of the two ciliated gills, which are also respiratory organs. Few papers have been published on the external and internal morphology of the gills of *G. veneriformis* L.

The optical observation of the gill structure and of the movement

of cilia of various marine mussels has been illustrated by Atkins (1936, 1937, 1938). Transmission electron microscopic studies of the gill of *Anodonta cataracta*, *Mytilus edulis* and *Basnea cadida* have been made by Gibbons (1961) and by Owens (1974). They described the fine structure of different portions of the cilium, the basal body, and the fibers associated with the basal bodies both in general and in detail. Moore (1971) and Owen (1974) examined the lateral frontal cirri and eu-latero-frontal cirri of *Mytilus edulis*, *Basnea cadida* and *Petricola pholadiformis* under scanning electron microscope. They emphasized the arrangement of the cilia which constituted the latero-frontal cirri and eu-latero-frontal cirri. Both Moore (1971) and Owen (1974) considered the small mesh sizes formed by the cilia of cirri to be correlated with the high retention of small particles in these filter feeders.

Recently, Lo and Hüber (1977 a & b) have described the gill of the lamellibranch molluscs, *Corbicula fluminea* Müller, as processing a highly specialized ciliary apparatus that consists of several distinct types of ciliated cell arranged in a regular manner. These ciliated apparatus on the gill filaments are involved in the movement of water, retention, sorting and transport of solid materials.

In the present study, both optical microscopy, scanning electron microscopy and transmission electron microscopy techniques were used to study the morphology of gills of *G. veneriformis* L. with the aim of investigating the structure and distribution of cilia and cirri on the gills, to understand the types of cilia on the gill filament of *G. veneriformis* as a basis for further work and histopathological study.

MATERIALS AND METHODS

Living specimens of the marine bivalve, *Gomphina veneriformis*, were obtained locally. The specimens were isolated and then treated with the following methods according to the apparatus used for observation.

For light microscopy, the whole specimens were fixed in Zenker's fixative, and processed for paraffin embedding. Dimensions were determined after fixation. Histological sections of 4 μ were stained with Mayer-haematoxylin and Eosin-Y. Observations were made with a bright field compound microscope.

For scanning electron microscopy, the gill was isolated from specimens from which one valve had been removed, and were placed in a small dish which was tilted so that a minimum volume of sea water was required to cover the surface of the uppermost gill. After being fixed for 20 min. in a formaldehyde-glutaraldehyde fixative, the gills were sufficiently hardened to be cut into suitably sized pieces and transferred to small stoppered vials for 3 hrs. Tissues were post-fixed in 1% osmic acid for 2 hrs., and then washed and dehydrated in a graded ethanol series (35-100%) before being dried in a CO_2 critical point apparatus. The deried specimens were coated with carbon and gold in that sequence. Micrographs were taken with the JSM-15 at 15 KV.

For transmission electron electron microscopy, the gills were also double-fixed with formaldehyde-glutaraldehyde and 1% osmic acid as in the procedure outlined above. After dehydration with the graded ethanol series, the specimens were embedded in Spurr Epon. Ultra-thin sections were made by glass knife and then double-stained with uranyl acetate and lead citrate. Observations and photographs were made with JEM 100 S at 80 KV.

OBSERVATIONS AND DISCUSSION

The bivalve, *Gomphina veneriformis* has a very solid, compressed and trigonal shell. The beak is situated at the middle of the dorsal margin. The surface is rather smooth and polished, and varies from white to blue in color, usually with 3 radial rays. The hinge plate has 3 solid cardinal teeth without laterals. The ventral margin is smooth. As in *Tapes japonica*, the orginal bluish tone of fresh shell is lost, turning into brown, when they are boiled to remove their soft body. The classification is as follows:

Phylum	Mollusca
Class	Pelecypoda
Order	Heteroconchia
Family	Veneridae
Genus	Gomphina

(1) General morphology of the gill

The gills of *G. veneriformis* are paired, each consists of two plate-like demibranchs hanging in the mantle cavity at either side of the food. Their filaments are bent back upon themselves like a "V", so that each of the demibranchs is double and composed of two flat lamellae. Each gill separately now forms a "W" in section. Each "V" of the "W" forms a demibranch; there are thus an inner and an outer demibranch, each two lamellae thick, in either gill. Two demibranches occur, the outer is smaller than the inner on each side of the foot.

Figure 1 is a scanning electron micrograph of the external surface of the outer gill. The surface of the gill is marked with dorsoventral folds plicae. On the surface of each plicae, there are many longitudinally parallel folds known as the the gill filaments (Figs. 1,2 & 9). The adjacent filaments are united by vascular cross connections, leaving narrow openings between them (Figs. 2 &3). The two lamellae of each demibranch become attached back to back in the same way.

The gill filaments are of two sorts: the smaller ordinary filaments and the larger principal filaments. About 12 to 26 ordinary filaments constitute each plicae fold, and the principal filament usually lies at the bottom of the crest groove (Fig. 2). Between the principal filaments of two lamellae, interlamellar junctions are present. The interlamellar junctions may be complete or incomplete (Fig. 2).

The ordinary filaments are uniform in size and lined with a continuous simple epithelium. As shown in Fig. 3, regional differentiation of the ordinary filament is readily evident. The front end of the filament is covered with simple columnar frontal cells (four cells)

with their frontal cilia. The cell is large and rich in acidophilic cytoplasm. The large ellipsoid nucleus runs parallel to the cell axis. The area adjacent to the frontal cell is lined with a simple ciliated columnar epithelium (eu-latero-frontal cell). The nucleus is large and oval. The cilia form triangular plates, probably from the fusion of several separated cilia. A row of lateral cells bears the lateral cilia just behind the lateral frontal edge. These pass the water current between the filaments, through the ostia, into the interlamellar space which leads above into the suprabranchial chamber, carrying water backwords towards the exhalant siphon. Its cytoplasm, like that of the eu-latero-frontal region, stains paler than that of the frontal region. The space between the lateral and eu-latero-frontal is demacrated with simple epithelium, devoid of cilia, the pro-lateral cell.

The adjacent filaments are united by vascular cross connections, leaving narrow openings between them. Water flows down through these openings into the interlamellar space. These pores called ostia, are not readily discernible in the scanning electron micrograph because their orifices are often covered with cilia and cirri (Fig. 3). Along the inner surface of the filamental epithelium, there are two cords of supporting structures. These supporting structures stain pale blue with H-E stain. The reaction indicates that the supporting structure may be chintinous (Figs. 3, 6 & 7). The specialization of the cell surface of the gill filament will be fully explored in the next section.

(II) The fine structure of the gill filament

The main part of the gill filament is covered with various cuboidal or columnar ciliated cells and secretory cells. There are great differences in size, shape, distribution and the surface modification. Figures 4 and 5 are diagrammatic representations of the cross sections of the gill filaments which may or may not have the sensory ciliary tufts. The filamental epithelium of both surfaces of the inner gill is similar to that of the external surface of the outer gill. There are 5 specialized surface modifications identified in these

regions. Most of the modifications are named according to their locations. The surface area of the distal end of the gill filament is divided into five regions: lateral, pro-lateral, eu-latero-frontal, pro-latero-frontal, and frontal. As shown in Fig. 7, six to seven ordinary cell types are found. They will be described in the following paragraph.

1. *The frontal cell*

There are four rows of simple ciliated columnar cells, 5.3μ×15.1μ in size, at the center of the frontal surface of the gill filaments (Figs. 6 & 7). Each frontal cell contains an ellipsoid nucleus, located at the base of the cell. The heterochromatin is concentrated to a thin rim near the nuclear envelope. Cytoplasm is very sparse, which is acidophilic with a limited number of spherical mitochondria. The part above the nucleus is occupied by numerous spherical, oval vesicles of variable size, clear or containing an electron-dense core. These structures may be part of a process such as phagocytosis (Fig. 8).

Numerous long, slender cilia extend from the apical surface of the frontal cells. Their distal ends intermingl with each other in an intricate mesh tilting ventrally (Figs. 10, 11, 12 & 13). Each cilia contains the typical 9+2 pattern of longitudinally arranged microtubules, originating from a basal body (Figs. 8 & 15). Frontal cilia are easily detached from the cell surface in treatment, revealing the underlying frontal cells. In the LM study, slime of mucus always appears to cover the entire frontal surface of each gill filament. But under scanning electron microscopic observation, few food particles are retained in this area. This would suggest that the frontal cilia play a role in propelling water current along the frontal surface. The slimy mucus could possibly provide a lubricating substratum for food transportation.

2. *pro-latero-frontal cell*

These cells are simple small, narrow elongated cells, arranged in a row along both slides of the frontal cells. The nucleus is elongated at the base of the cell, with a thin marginal zone of dense heterochromatin and several nucleoli. The acidophilic cytoplasm is filled

with a varied number of vesicles, lysosomes and residual bodies. Most of the vesicles are smooth but some are typically coated. A limited number of Golgi apparatus is located in the vicinity of the nucleus, with some parallel saccules and vacuoles. Small membrane-bounded granules may be present near the Golgi zone. The mitochondria are round but scarce.

The pro-latero-frontal cilia are arranged on each side of the frontal cilia. (Fig. 12) They are shorter and always obscured by the frontal cilia and eu-latero-frontal cirri. As shown in Figs. 13 & 19, cilia are laid open to view in some area but partially sheltered in others. The cilia are characterized by its expanded distal tip into a disc-shaped (Fig. 14). This structures probably act as a second sieve, preventing the escape of small particles between the bases of the eu-latero-frontal cirri.

3. *Sensory ciliary cell*

These cells with dense tufts of cilia are occasionally interspersed at intervals along the rows of pro-latero-frontal cells (Fig. 9). These cilia are considerably larger and they project above the frontal and eu-latero-frontal cirri (Figs. 10 & 16). Such tufts were noted by Atkins (1937), who concluded that they were probably sensory in function. It is perhaps significant that at least in *G. veneriformis*. They are irregularly distributed on each lamella of the demibranch (Fig. 1).

4. *eu-latero-frontal cell*

There is a row of larger columnar cells just on each side of the pro-latero-frontal cells of the gill filament (Fig. 6). The ellispoid nucleus at the basal part is also larger than that of the frontal cell. Chromatin are loosely distributed; large and coarse granular nucleoli are characteristic of it (Fig. 7). The cells contain a relatively large number of oval mitochondria, most of which are clustered in the apical part (Fig. 7). The cytoplasm is acidophilic. There is a large Golgi zone, some profiles of granular endoplasmic reticulum, ribosome and lysosomes both primary and secondary. Occasional tonofilaments occur. Each cilium contains longitudinally arranged microtubules: two single in the center and nine double in the

periphery. The latter emanate from nine triple microtubules in the basal bodies just below the cell surface. The basal bodies posses longer ciliary rootlets and often lateral spurs. A network of cytoplasmic filaments interconnect the ciliary rootlets (Fig. 6). This may account for the synchronization of ciliary beat within the restricted area.

The eu-latero-frontal cirri is borne by a single cell and consists of two parallel but alternating rows of cilia (Figs. 19 & 20). Each cilium is divided into two parts, a free marginal part and a fixed basal part (Figs. 17 & 18). The individual cilium comprising each cirrus diverge from the main axis of the cirrus at intervals to form side "branches". The divergence is first shown by the two cilia nearest the frontal surface of the filament, the shortest cilia comprising the cirrus, while the distal end of the cirrus is formed by the divergence of the two cilia farthest from the frontal surface, that is the longest cilia. The basal part of each cilium adheres side by side in a triangular basal sheet resting on the edge of the frontal surface. The basal sheet of the eu-latero-frontal cirrus is flexible.

Each cirrus forms a flexible comb, the free region of each cilium bends to one or the other side of the main axis of the cirrus (Fig. 18). This bending occurs at regular intervals along the length of the cirrus which ends with a bifuraction formed by the separation of the longest pair of cilia. The overal effect is to produce a meshwork right across the water space, straining off particles for retention on the frontal surface of the gill. This prevents the unimpeded passage of particles from the gill filaments to the supra-branchial chamber and contributes to the high efficiency of the method of feeding, preventing the escape and wastage of perhaps desirable food particles.

5. *pro-lateral cell*

Between the lateral cells and the eu-latero-frontal cells is a row of non-ciliated pro-lateral cells. The cell is low columnar, averaging $7.6\,\mu \times 10.2\,\mu$. It has a round nucleus in the central area. The cytoplasm is abundant and contains a moderate amount of free ribosomes and granular endoplasmic reticulum. The Golgi zone is prominent

with numerous vesicles of both the smooth and the coated variety. Mitochondria are oval but few in number. From the cell surface are projected a large number of short, differently shaped microvilli (Figs. 6 & 7). The microvilli serve the purpose of increasing the absorptive area, but in the scanning electron microscopic study they are obscured by other elongated surface specializations. The surface membrane has dense pinocytotic invagination, most are smooth, but some are typical coated. The cells are filled with a varied number of vesicles, vacuoles, lysosome and residual bodies. These structures are part of a process referred to phagocytosis.

6. *lateral cell*

Baside the pro-lateral cell, there are 3 rows of cells bearing the long lateral cilia. Those nearest to the pro-lateral cell are wider and shorter with a round nucleus at the central part; the other two row cells are especially long and narrow with a slender elongated nucleus at the basal part (Figs. 6 & 7). The cytoplasm is pale staining with acidophilic nature, and filled with numerous spherical mitochondria with diameter averaging 0.9 μ. The mitochondria are closely packed with membraneous cristae. This gives the lateral cell a high rate of oxidative metabolism. There are only a few dense matrices in the mitochondria.

The lateral cilia are very long; below the cell surface, the basal bodies possess short ciliary rootlets and often lateral spurs. The cilia are rarely observed in scanning electron microscope because they hide in the groove-formed by the adjacent gill filaments (Figs. 19 & 20). The long lateral cilia within the grooves may serve to drive water between gill filaments and maintain currents of water flowing toward the gill surface.

The 5 different functions of the groups of cilia bent anteriorly and posteriorly along the margin of the gill transport either collected food to the labial palps (in oral grooves) or rejected particles backwards. Such currents run in grooves along the demibranch margin or dorsally at the inner or outer base of the gills. Particles are brought to them by the frontal cilia beating up or down the filaments.

The filtering power of the gill may be varied by altering the width of the ostia or the speed of the current. A typical lamellibranch filters thirty to sixty times its own volume of water in a hour. As the water passes between the filaments, food particles are held back by straining cilia and are carried forward by other cilia in mucous strings towards the mouth; filtration is probably chiefly the function of the eu-latero-frontal cilia.

ACKNOWLEDGEMENT

This work was supported in part by a grant from the Society of the Divine Word research Fund. Their assistance is gratefully acknowledged.

REFERENCES

(1) D. Atkins, *Q. J. Microsc. Sci.* 79, 181 (1936).
(2) D. Atkins, *Q. J. Microsc. Sci.* 79, 339 (1937).
(3) D. Atkins, *Q. J. Microsc. Sci.* 79, 375 (1937).
(4) D. Atkins, *Q. J. Microsc. Sci.* 80, 330 (1938).
(5) D. Atkins, *Q. J. Microsc. Sci.* 80, 346 (1938).
(6) I. R. Gibbons, *J. Biophys. Biochem. Cytol.* **11**, 179 (1961).
(7) C. F. Lo and F. Hüber, *Proc. Nat. Sci. Cou.* 10, 361 (1977).
(8) C. F. Lo and F. Hüber, *Fu Jen Studies* **11**, 55 (1977).
(9) H. J. Moore, *Mar. Biol.* **11**, 23 (1971).
(10) G. Owen, *Proc. R. Soc. Lond. B.* 187, 83 (1974).

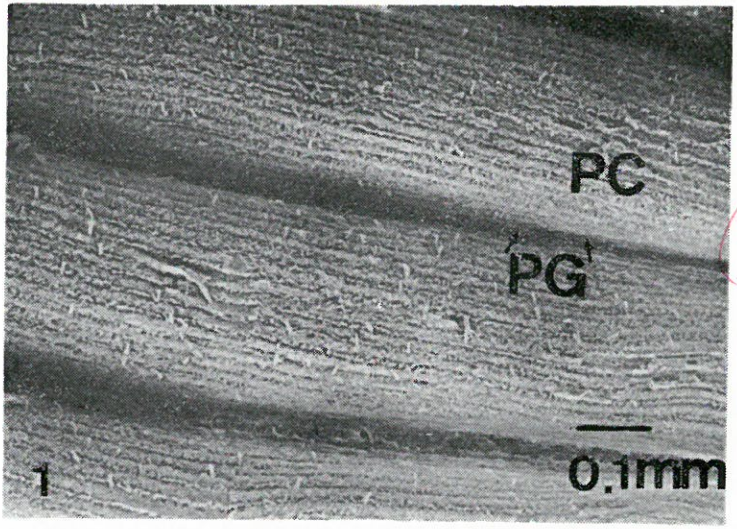

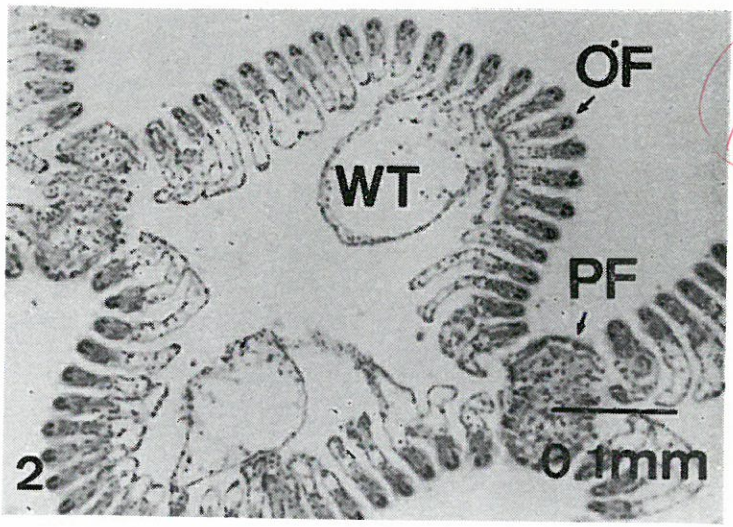

Fig. 1. A scanning electron micrograph of the external surface of the gill plate.
PC: plical crest PG: plical groove

Fig. 2. A light micrograph of a cross section of a gill plate, showing the ordinary gill filaments on the crest, and principal gill filament on the groove.
OF: ordinary filament WT: water tube
PF: principal filament

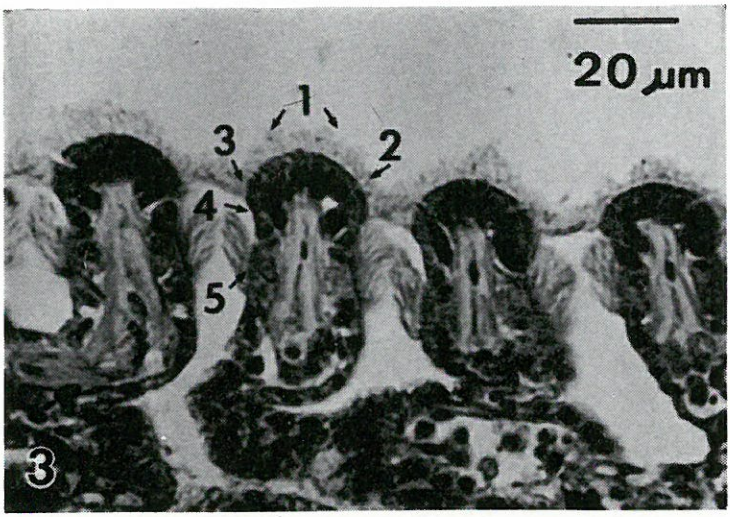

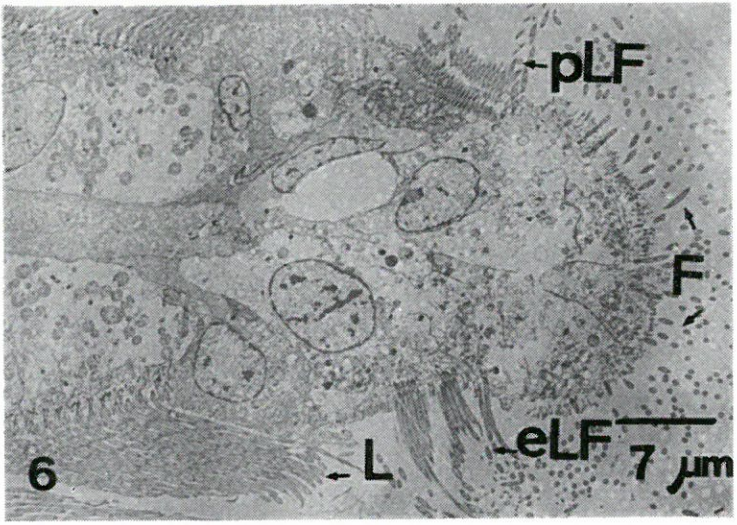

Fig. 3. A light micrograph of a cross section of gill plicae, showing the regional differentiation of gill filament.
1. frontal region
2. pro-latero-frontal region
3. eu-latero-frontal region
4. pro-lateral region
5. lateral region

Fig. 6. A transmission electron micrograph of a cross section through a gill filament.
F: frontal cilia
eLF: eu-latero-frontal cirri
pLF: pro-latero-frontal cell
L: lateral cilia

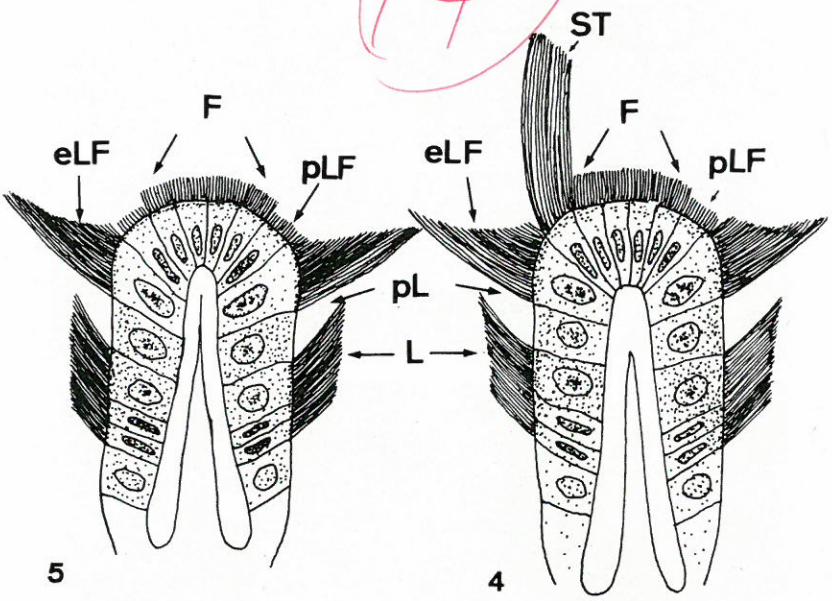

Fig. 4. Diagrammatic drawing of a cross section of external lamella filament showing the arrangement of cells.

Fig. 5. Diagrammatic drawing of a cross section of internal lamella filament showing the arrangement of cells.

F: frontal cilia
eLF: eu-latero-frontal cirri
pLF: pro-latero-frontal cilia
pL: pro-lateral cells
L: lateral cilia
ST: sensory ciliary tufts

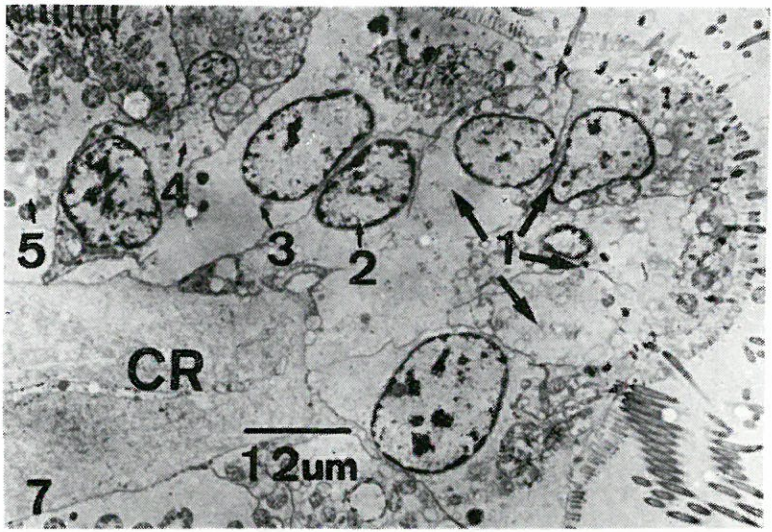

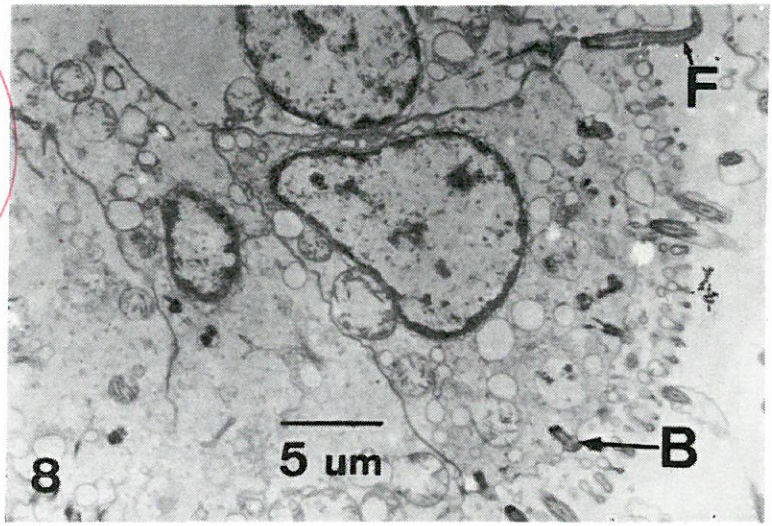

Fig. 7. A transmission electron micrograph of a oblique cross section through a gill filament, showing the various cell types of the gill epithelium.
1. frontal cell
2. pro-latero-frontal cell
5. eu-latero-frontal cell
4. pro-lateral cell
5. lateral cell
CR: chintinous rod

Fig. 8. A transmission electron micrograph of a surface of gill epithelium, showing the fine structure of the frontal cells.
F: frontal cell BD: basal body

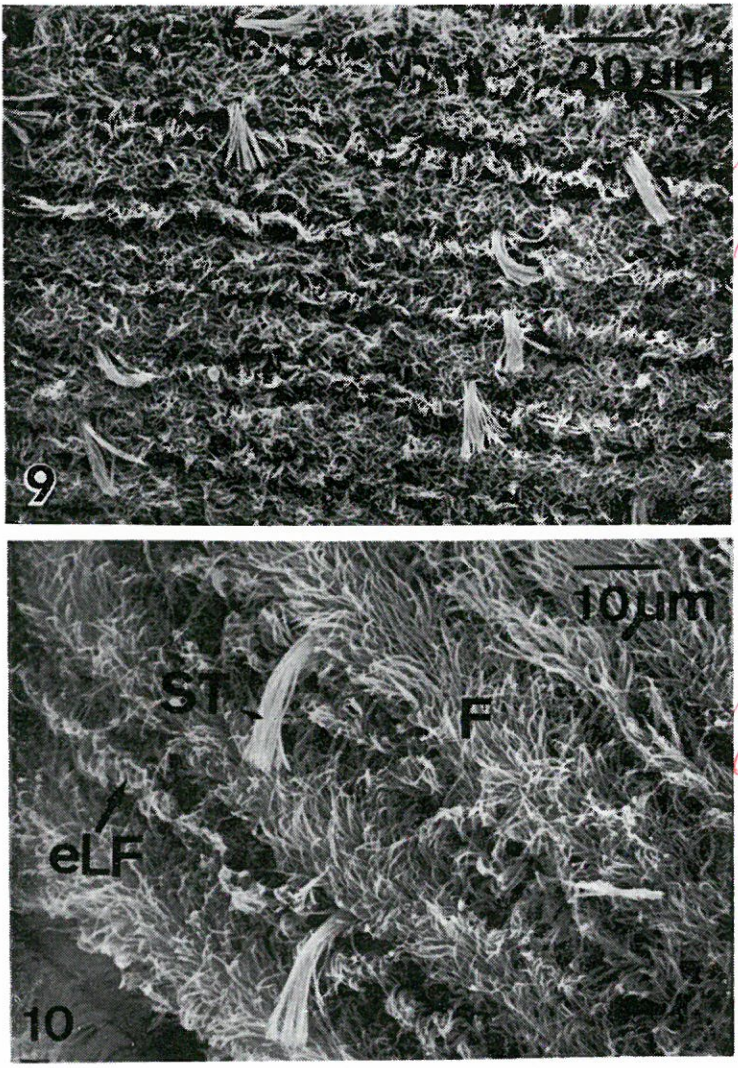

Fig. 9. A scanning electron micrograph of the enlargement of Fig. 1, showing the various groups of cilia that cover the plical crest.

Fig. 10. A scanning electron micrograph of the gill filament, showing three complete sets of cilia on the gill filaments.
F: frontal cilia ST: sensory ciliary tufts
eLF: eu-latero-frontal cirri

Fig. 11. A scanning electron micrograph of the gill filament, showing the frontal cilia and the flexible eu-latero-frontal cirri.
F: frontal cilia ST: sensory ciliary tufts
eLF: eu-latero-frontal cirri

Fig. 12. A scanning electron micrograph of the frontal view of the gill, showing the pro-latero-frontal cilia projecting between the cilia and eu-latero-frontal cirri.
F: frontal cilia eLF: eu-latero-frontal cilia
pLF: pro-latero-frontal cilia ST: sensory ciliary tufts

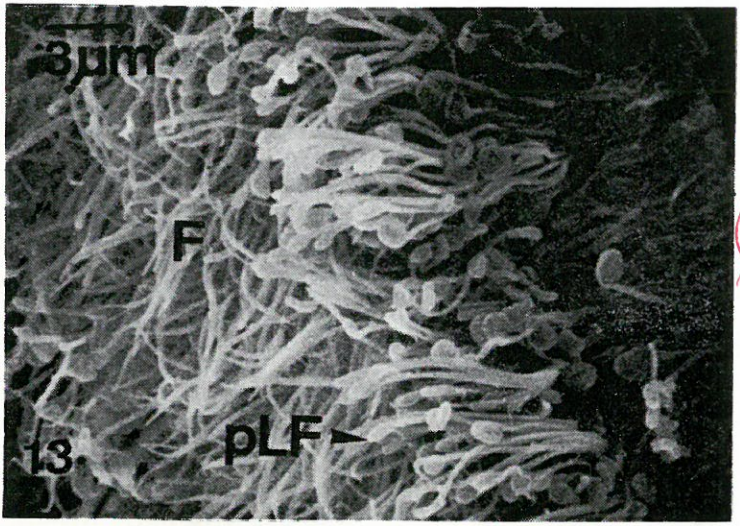

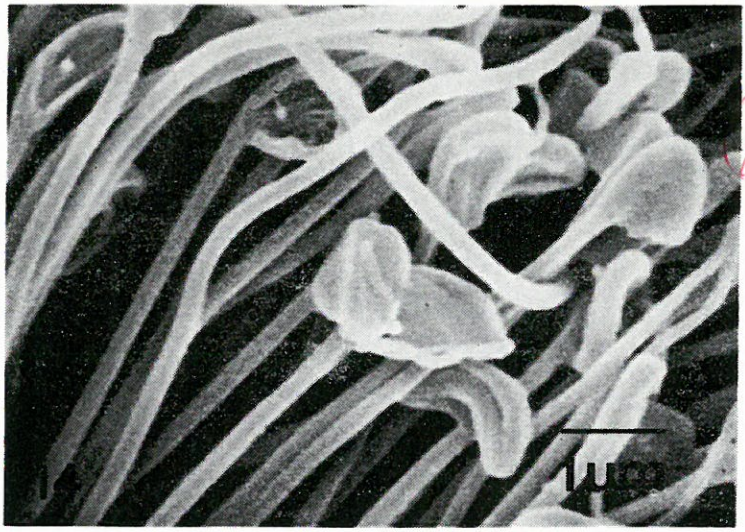

Fig. 13. A scanning electron micrograph of the ab-frontal view of the pro-latero-frontal cilia, which set beside the frontal cilia.
F: frontal cilia pLF: pro-latero-frontal cilia

Fig. 14. A scanning electron micrograph of the enlargement of Fig. 13, showing the pLF with the disc-shaped end.

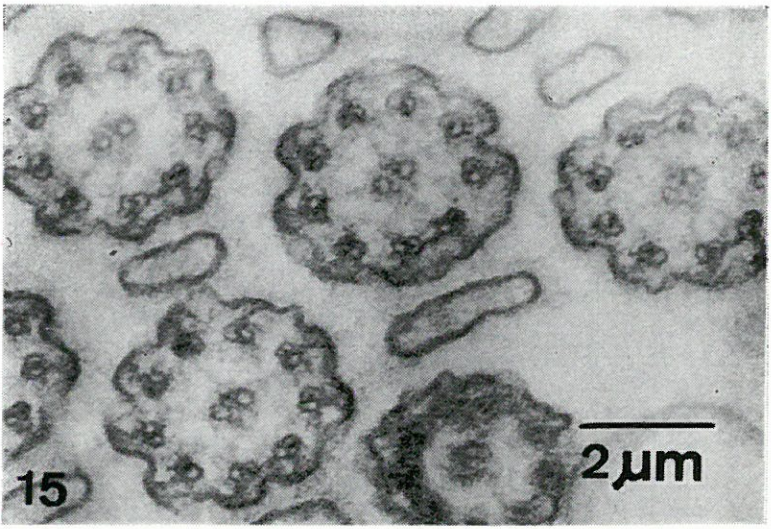

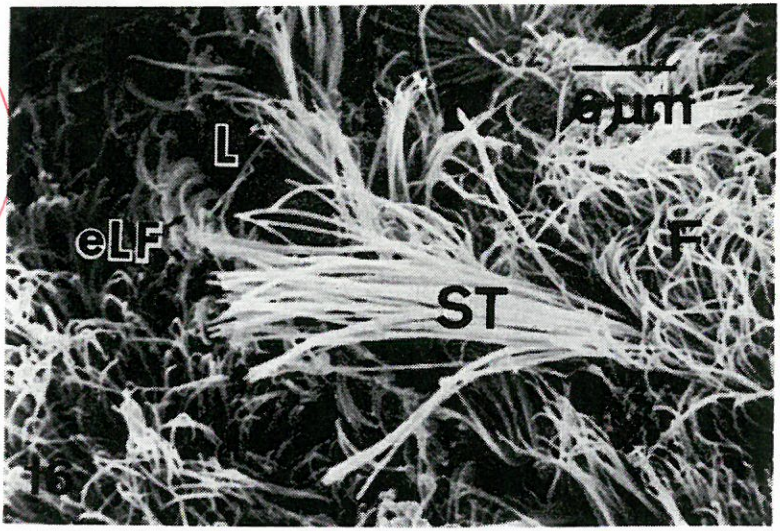

Fig. 15. A transmission electron micrograph of the cross section through the frontal cilia, showing the 9+2 pattern.

Fig. 16. A scanning electron micrograph of the frontal view of the gill filament, showing:

F: frontal cilia
L: lateral cilia
eLF: eu-latero-frontal cirri
ST: sensory ciliary tufts

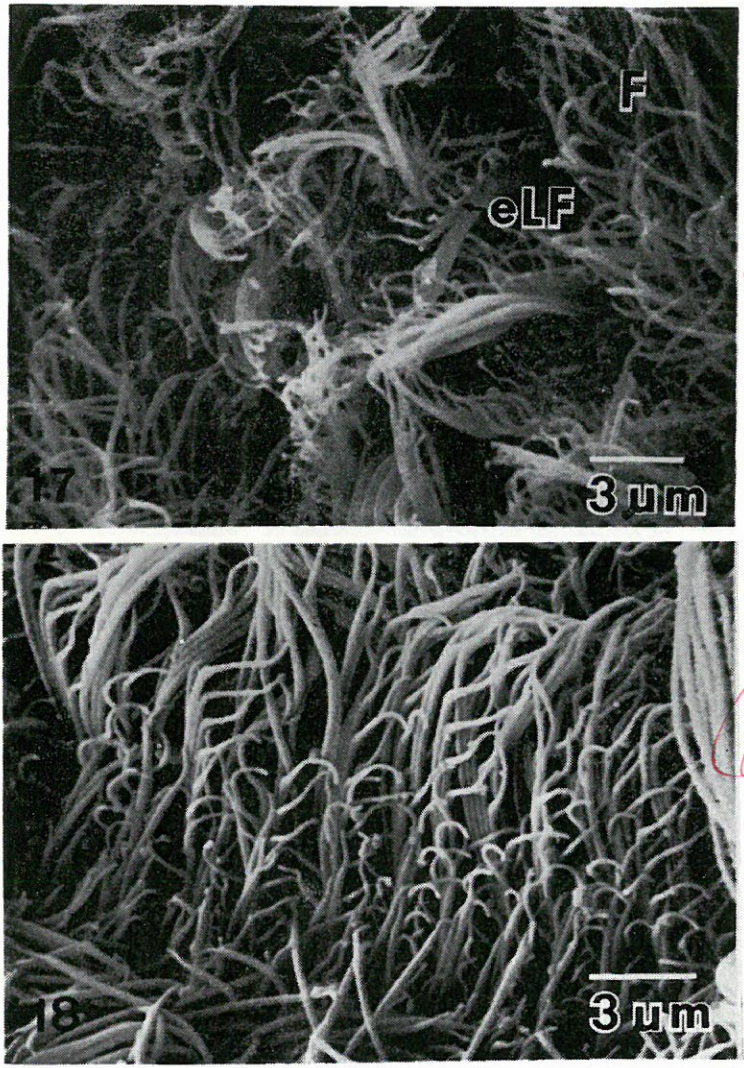

Fig. 17. A scanning electron micrograph of the eu-latero-frontal cirri of two adjacent fill filaments, showing the mesh formed by the divergence of the cilia comprising the main axis of each cirrus.
F: frontal cilia eLF: eu-latero-frontal cirri

Fig. 18. A scanning electron micrograph of the later-abfrontal view of the eu-latero-frontal cirri, showing the free marginal part and the fixed baasal part of the cirri.
eLF: eu-latero-frontal cirri

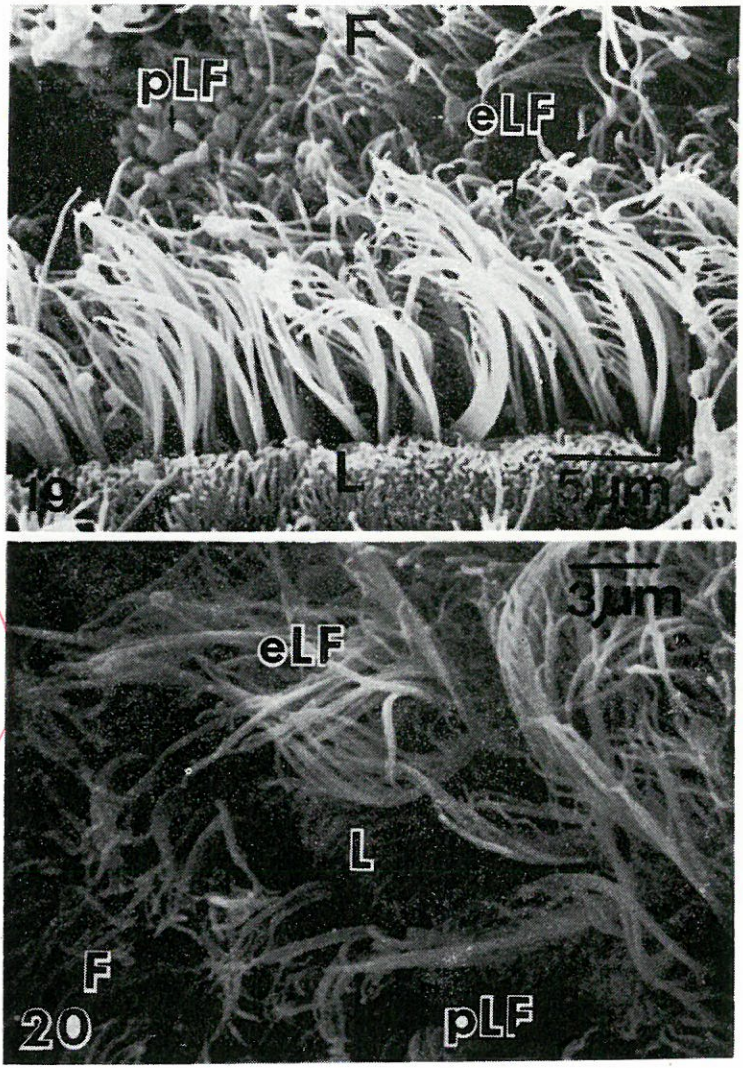

Fig. 19. A scanning electron micrograph, showing the eu-latero-frontal cirri bending to the frontal surface on the gill filament.
F: frontal cilia eLF: eu-latero-frontal cirri
pLF: pro-latero-frontal cilia L: lateral cilia

Fig. 20. A scanning electron micrograph, an enlargement of Fig. 11, showing the lateral cilia hidden in the gill groove.
F: frontal cilia pLF: pro-latero-frontal cilia
eLF: eu-latero-frontal cirri L: lateral cilia

花蜊之組織及病理研究

崔 文 慧

生物系

摘 要

花蜊屬軟體動物門、斧足綱，爲濾食性動物：鰓絲表面至少有五種纖毛，呈規則分佈。纖毛的種類與分佈方式，關係其水流方向，食物的運送與攝取，殘渣的排除等。

本實驗應用掃描式及穿透式電子顯微鏡，研究花蜊鰓之細微構造，以期作爲更進一步病理研究之依據。

葡萄酵素性褐變之研究

II. 金香葡萄於發育與成熟過程中聚酚氧化酶活性之變化

食品營養研究所

陳雪娥　金蘭馨

摘　要

本研究就金香葡萄於不同的栽植地區與季節，其果實成熟過程中聚酚氧化酶（PPO）活性的變化作一探討。結果發現，成熟之冬季金香葡萄可溶性固形物及可滴定酸度比夏果高；隨着發育成熟過程 PPO 活性呈上下浮動之不穩定的現象，但至成熟期冬果之 PPO 活性比夏果略低，而二林地區金香葡萄之 PPO 活性略高於后里地區的葡萄。

引　言

酵素性褐變與原料之聚酚氧化酶（PPO）活性及酚化物含量有密切關係[4,7]。歐美栽培的葡萄 PPO 活性在葡萄成熟期逐漸增加，有的品種在成熟採收時，活性達到頂點，過熟則活性降低；有些品種 PPO 之活性在成熟前一週至二週活性最高，採收時活性已下降。由文獻顯示，在相同栽培條件下，同一品種不同年度收成，PPO活性也有變化，此可能與氣候有關[5,6]。臺灣金香葡萄生長期與歐美栽種的情形不同。歐美葡萄於七至九月間生長、成熟，此時期氣溫逐漸轉涼。臺灣金香葡萄一年有兩穫、夏季生長成熟期在五至七月，氣溫爲逐漸上升；而冬季生長成熟期在九月至十二月，氣溫漸低。因此兩者在成熟過程中 PPO 活性的變化是否一樣呢？地區性是否會有不同的變化呢？這將是本實驗探討的主要目的。

材料與方法

試驗材料採自臺中縣后里鄉及彰化縣二林鎭葡萄專業區之果園。採樣時期爲1984年 5 月至 7 月（夏季）及 9 月至12月（冬季）。金香葡萄開花着果後，選擇果穗大小一致者，在果實發育期，每隔兩週採樣一次。成熟期則每隔 7 至10天採樣，直到葡萄成熟採收。取樣時，每次摘 6 穗的葡萄，其中兩穗直接供分析可滴定酸度（titratable acidity）及可溶性固形物（soluble solids）用。另外 4 穗摘下後立刻放入乾冰箱冷凍，供分析 PPO 活性用。

利用均質機將葡萄以 5,000×g 轉速打碎 1 分鐘，但不破壞種子。碎果經四

層紗布過濾，得果汁供可滴定酸度[3]及可溶性固形物[3]之分析。

冷凍葡萄加2倍體積之丙酮（−20°C）及1% PEG（分子量 6,000），以5,000×g 轉速，在 0°C 冰浴均質1分鐘。經 Toyo 1 號濾紙減壓過濾，並剔除種子。沈澱物依上法重覆萃取三次之後，置於室溫下蒸發丙酮，再移入乾燥器內乾燥，可得丙酮粉（aceton powder）。丙酮粉加100倍之 pH 7.0 緩衝液（含1M 氯化鉀、0.05M 硫酸氫二鉀，4°C），混勻，置入 4°C 冰箱中，振盪之。三小時後經高速冷凍離心（12,000 ×g）15分鐘。上層液經玻璃棉過濾，即爲粗酵素液。PPO 活性之測定是參考 Wissemann 及 Lee (1981)[8] 的方法，以兒茶酚（catechol）爲作用基質，pH 6.5 之 MacIlvain 爲緩衝液，測波長 420 nm 吸光度之變化量，計算 PPO 活性。將每分鐘吸光度增加 0.001 A 訂爲1單位（unit），以 unit/berry 及 unit/g fresh deseed grape 表示 PPO 活性。

結果及討論

一、金香葡萄發育過程中可溶性固形物及可滴定酸度之變化

圖1及圖2爲后里及二林兩地之金香葡萄，在1984年夏季及冬季果實發育成熟過程中，可溶性固形物及可滴定酸度之變化情形。無論冬季或夏季果實的發育初期可溶性固形物含量極低，增加的也很緩慢，幾乎呈一平穩狀態。當葡萄開始軟化，也就是進入成熟期後（約在開花着果後50天），可溶性固形物含量急增，

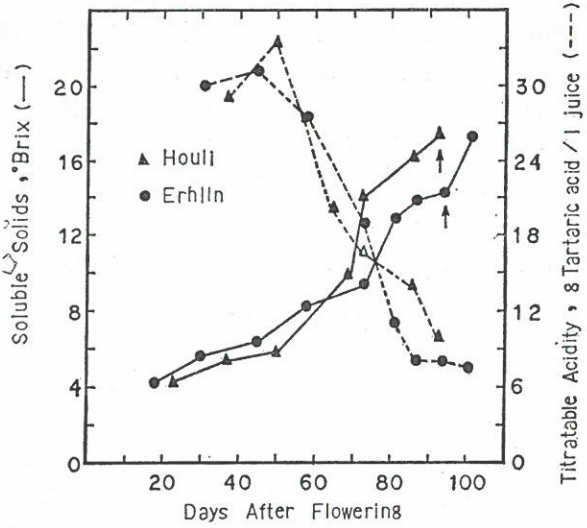

Fig. 1. Changes of soluble solids and titratable acidity during development and maturation of Golden Muscat grapes in summer of 1984.

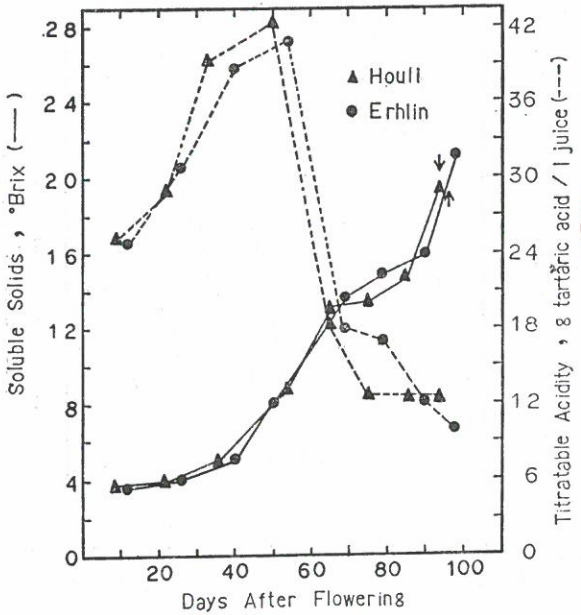

Fig. 2. Changes of soluble solids and titratable acidity during development and maturation of Golden Muscat grapes in winter of 1984.

直到成熟末期。過熟之葡萄（二林，夏季）可以明顯地看出果皮皺縮，可溶性固形物有增加的現象。比較夏季及冬季果實內可溶性固形物含量，顯示冬果之含量較高。此乃因冬果受氣溫之影響，呼吸作用低，能量消耗少，故可溶性固形物含量較夏果爲高。

可滴定酸度與可溶性固形物含量的變化相反。在果實發育後，可滴定酸度即迅速上升，直到硬核期之末，有機酸累積到最高量，然後迅速下降，於成熟末期降至最低。冬季及夏季可滴定酸度之變化型態相似。葡萄中的有機酸主要包括酒石酸及蘋果酸[1-3]。酒石酸合成於果實初生期，在整個發育成熟過程，其含量維持穩定，變化不大。可滴定酸度的變化，主要來自蘋果酸含量的波動，當氣溫高時，蘋果酸代謝快，果實中的含量因而降低，葡萄汁的可滴定酸度也下降[1]。夏季葡萄的發育成熟期自 5 月至 7 月底，氣溫逐漸昇高；而冬季葡萄的發育成熟期在 9 至12月間，果實在氣溫日漸下降的環境下成熟，因此冬季採收之成熟葡萄含酸量較高。若以酒石酸表示葡萄中的含酸量，后里夏果果汁每 *l* 含 10 g 可滴定酸，較冬果之 13 g 爲低。二林夏果每 *l* 果汁含 8 g 可滴定酸較冬果之 11 g 爲低。若以兩地區比較，二林之冬、夏果含酸量皆低於后里的。

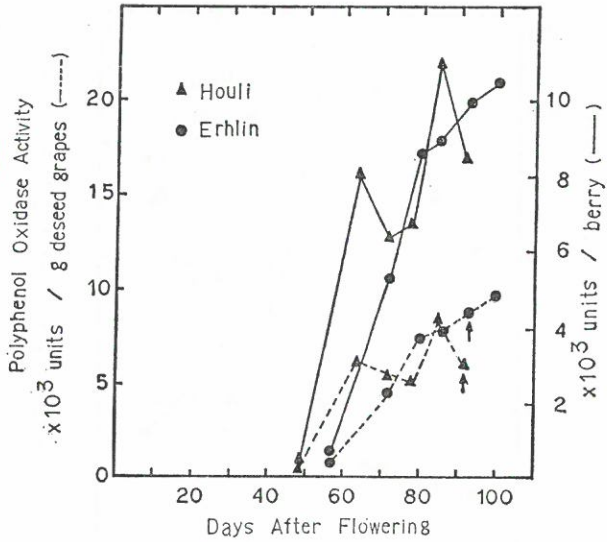

Fig. 3. Activities of polyphenol oxidase of Golden Muscat grapes during development and maturation in summer of 1984.

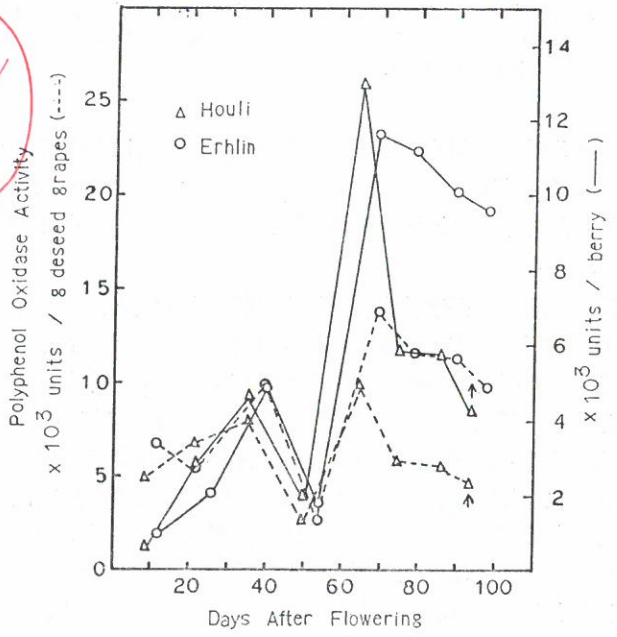

Fig. 4. Activities of polyphenol oxidase of Golden Muscat grapes during development and maturation in winter of 1984.

二、金香葡萄發育成熟期間 ppo 活性之變化

1984年夏季，后里及二林地區金香葡萄成熟期間 PPO 活性的變化顯示於圖3。無論是以單粒重或鮮重計算 PPO 活性，自成熟期開始，二林地區葡萄的 PPO 活性急速上升，至成熟末期活性才增加減緩。圖中箭頭所指爲採收時之活性，二林過熟的葡萄 PPO 活性仍繼續上升。后里地區的葡萄其 PPO 活性變化較不規則，但至成熟末期有下降的現象。

在冬季，后里及二林之金香葡萄 PPO 活性變化有相同趨勢，如圖4。在果實初生期(0～30天)，單粒果實 PPO 活性增加迅速，直到硬粒期之初，PPO 活性達到頂點，隨後迅速下降，當果實進入成熟期（開花後50天）PPO 活性又大幅增加，隨後，兩地區葡萄之 PPO 活性皆下降。以成熟採收的葡萄果實而言，后里地區之葡萄 PPO 活性低於二林地區的。由成熟期之 PPO 活性變化情形來看，后里與二林地區葡萄 PPO 活性皆呈下降趨勢，與這段期間氣溫日趨寒冷似乎有關。歐美等國栽種的葡萄發育成熟期自6月至10月氣溫與臺灣之冬果發育成熟期較接近，許多品種葡萄之 PPO 活性大都在氣溫已轉涼的10月中旬開始下降[6,7]。

比較兩地區夏季與冬季成熟金香葡萄 PPO 活性，可看出后里冬季每單位鮮重葡萄 PPO 活性比夏季低。二林之冬夏果則幾乎相同。但對單粒葡萄而言，后里夏果 PPO 活性高達冬果的2倍。以地區而言，后里之葡萄 PPO 活性皆比二林低，尤其是冬果差異更顯著。

由以上可歸納出，在氣溫逐漸上升的夏季成熟期，金香葡萄 PPO 活性也隨之上昇；而天氣轉涼的冬季，PPO 活性也逐漸下降，此可能是受氣溫高低的影響。至於褐變情形及不同年度是否有相同的變化現象，則有待進一步研究。

參考文獻

(1) 何妙瀚，臺灣冬季釀酒葡萄酸度偏高之生理探討。碩士論文。國立中興大學園藝研究所。(1983)。
(2) D. E. Carroll and J. E. Marcys, *Am. J. Enol. Vitric.* 33, 168 (1982).
(3) L. A. Johnson and D. E. Carroll, *J. Food Sci.* 38, 21 (1973).
(4) V. Kahn, *J. Food Sci.* 42, 38 (1977).
(5) A. M. Mayer and E. Harel, *Phytochemistry* 18, 193 (1979).
(6) J. C. Sapis, J. J. Macheix and R. E. Cordonnier, *J. Agric. Food Chem.* 31, 342 (1983).
(7) K. W. Wissemann and C. Y. Lee, *Am. J. Enol. Vitic.* 31(3), 206 (1980).
(8) K. W. Wissemann and C. Y. Lee, *Food Sci.* 46, 506 (1981).

Studies on the Enzymatic Browning Capacity of Grapes II. Changes in Polyphenol Oxidase Activities During Development and Maturation of Golden Muscat Grape

HSUEH-ERR CHEN and LAN-SHIN CHIN

Gradute Institute of Nutrition and Food Science

ABSTRACT

Changes in polyphenol oxidase (PPO) activity during development and maturation of Golden Muscat grape from two growing seasons and two production areas were studied.

The results showed that mature winter grapes were higher in total soluble solids and titratable acidity than summer grapes. The PPO activities of both summer and winter grapes fluctuated during stages of development and early maturation. But at the mature stage, winter fruits were lower in PPO activity than summer fruits. The grapes from Erhlin showed a higher PPO activity than those from Houli.

ABSTRACTS OF PAPERS BY FACULTY MEMBERS OF THE COLLEGE OF SCIENCE AND ENGINEERING THAT APPEARED IN OTHER JOURNALS DURING THE 1985 ACADEMIC YEAR

Classical Trajectory Calculations for Atom (Ion)-Diatomic Scattering

FRANK E. BUDENHOLZER

Proc. Natl. Sci. Counc. ROC(A), Vol. 9, No. 4, 1985, pp. 312-325

Classical trajectory calculations provide an important technique to model both reactive and nonreactive atom (ion)-diatiom collisions. If the potential energy for all accessible atomic configurations is known (potential energy surface) and if the initial positions and velocities of the particles are defined, then the classical equations of motion can be numerically integrated to give the positions and velocities at all future times. This review will focus on work carried out in our laboratory under the sponsorship of the National Science Council. We first review some basic concepts and their application in the study of spherically symmetric systems. Rotationally inelastic, nonreactive scattering is then considered with special emphasis on the use of classical perturbation scattering theory to study ion-diatomic collisions. We then consider reactive scattering and discuss our recent work on the $F+H_2$ reaction. The paper closes with a few remarks on the relationship between classical and quantum mechanical methods.

Comparison of the Ease of Thermolysis of Ortho-Substituted Phenyl Azides Having α, β or β, γ Imine Functions

SHANG-SHING P. CHOU, PETER A.S. SMITH,* and GREGORY F. BUDDE*

J. Org. Chem., 1985, 50, 2062-2066

o-Azidobenzaldehyde benzylimine (7) thermolyzes 34 times faster than phenyl azide and 1.6 times faster than *p*-chlorobenzaldehyde *o*-azidoanil (8), whereas benzaldehyde (*o*-azidobenzyl)imine (9) and acetophenone (*o*-azidobenzyl)imines (10a-e) show little or no rate enhancement over phenyl azide. An electrocyclic mechanism can account for the rates of 7 and 8 relative to each other but not of 8 relative to phenyl azide; 9 and 10a-e appear to thermolyze by nitrene formation, even though a mechanism through intramolecular cycloaddition may in principle be available. A mechanism based on electrostatic effects in a dipolar transition state can correlate the effects of different types of α,β-unsaturated ortho substituents.

* Department of Chemistry, The University of Michigan, Ann Arbor. Michigan 48109.

Levels of Isozyme Variation Within and Among *Histoplasma capsulatum* Localities

C. LAN, J.L. HAMRICK* and R.W. LICHTWARDT*

Transactions of the Kansas Academy of Science,
89(1-2), 1986, pp. 49-56

Electrophoretic data from four *Histoplasma capsulatum* Darling sites was reanalyzed to determine the distribution of phenotypic variation within and among localities and individual soil samples taken from the localities. Three of the United States localities were blackbird roosts while the fourth was a gull nesting area. These results were compared to those from a third substrate type—a bat cave located in Colombia, South America. Approximately 48% of the total phenotypic diversity in six enzyme systems was found within an individual soil sample, 27% occurred among samples within localities and 25% occurred among localities. The Colombian bat site was not exceptional in terms of phenotypes observed or phenotype frequencies. However, this locality had less heterogeneity among soil samples than did the bird sites.

* Department of Botany, University of Kansas, Lawrence, Kansas 66045.

The Studp of *Clinostomum complanatum* (RUD., 1814) V. The Influences of Metacercaria of *Clinostomum complanatum* on Fish

Chu-Fang Lo, Shih-Chieh Chen and Chung-Hsiung Wang

Fish Pathology, 20 (2/3) 305-312, 1985. 9

Microscopically, the metacercariae of *Clinostomum complanatum* were encapsulated by a fibrous layer to form a cyst. The cyst wall was composed of connective tissue fibers, chiefly collagen fibers, of the fish in reaction to the infection. There were blood vessels penetrating into the cyst wall and forming a capillary network. These blood vessels might supply the nutritional requirements of the metacercaria and remove the wastes produced by the worms.

The metacercaria of *C. complanatum* got a lot of nutrients from its host for growth and storage. The possible routes of the metacercaria of *C. complanatum* to get nutrients from its host may be through the digestive tract or by the direct absorption of the covering of the worm from the body fluid of the fish. The morphological feature suggested that the tegument of the metacercaria of *C. complanatum* possessed the tegumental absorption function.

Generally, the metacercariae of *C. complanaium* lay quiescently in the cyst. No great harm was done to fish unless there were massive numbers. The greatest damage occurred when metacercariae had been activated and migrated out of the body wall of the fish. The process of the excystment and migration of the worms caused the congestion and hemorrhage followed by the serious tissue damage. After the excystment of the metacercaria, the fish tissues around the worm were dissolved. The result indicated that the worm might produce certain enzymes to facilitate the dissolution of fish tissues and cause the death of the fish due to the destruction of the fish body.

A Very Compact Chinese System Using Component Method and Character Generator

YEONG-WEN HWANG

Proceeding of the 1985 International Conference on
Chinese Computing, San Francisco,
February 26-28, 1985

This paper describes a microcomputer using component(radical) method and character generator to process Chinese. With new keyboard design which assigns components to a new alphabetic keyboard, separate component keyboard may be omitted. The whole system is integrated inside the keyboard.

A text editor operating in both screen mode and command mode was written for easy editing work of the mixed Chinese and alphanumeric text. Beside unlimited number of characters, the system can handle CAI lessons, games and BASIC in Chinese.

State-Space Approach to the Analysis and Design of A Synchronous Phase Convertor

C. H. LIU* and Y. S. LEE

IEE Proceedings. Vol. 132 Pt. B No. 3, p. 164-170, May, 1985

The state-space model of a synchronous phase convertor is formulated by using the nonlinear dynamic equations of both the pilot (Synchronous) and the load (induction) motors. A design proceedure is presented for computing the parameters of a linear controller for the field exciter of the synchronous motor. The controller parameters are updated according to the selected steady-state operating conditions. The proposed controller is suitable for microcomputer implementation. The validity of the controller design method is further verified by using computer simulation. Numerical experiments indicate that the synchronous phase convertor system can be operated stably under different load andfault conditions.

* Departement of Electrical Ergineering and Technology. National Taiwan Institute of Technology.

Play and Social Development in Taiwan

SHU-FANG LO CHIA

Joe L. Frost and Sylvia Sunderlin, eds.
From When Children Play, Association
for Childhood Education International
Wheaton, MD, 1985, pp. 61-65

Many kinds of play may be traced back to early years of the Han Dynasty (206 B.C..-219 A.D.) such as Dragon dance and the Lion dance; puppet show and shuttle-cocks; jumping rope and flying kites; swinging and hopescotch; playing with bamboo and paper toys; paper cutting; chio-lian huan (mathematical training) diagrams, playing with kaleidoscopes and bamboo instruments. Through such play activities, children can experience a wide variety of the elements of cultural and traditional play.

Contemporary preschool children's play, school-age children's play and childhood groups. As the child grows older and more experienced, playful treatment of toys becomes more diverse and sophisticated. Both imagination and intellectual curiosity begin to contribute to play. After entering school, most children want companionship. They become interested in games, sports, hobbies and other more mature forms of play. The quality of school children's play becomes more social.

School Children achieve acceptance in a group and, with cooperative play activities, an opportunity to learn to play in a social way.

Play contributes to children's social development and the development of desirable personality traits and social adjustments.

熱殺菌條件對百香果汁品質之影響

方祖達 邱美珠 陳雪娥

食品科學 第十二卷 第三、四期 第87-99頁 七十四年

影響百香果汁品質之因子很多，諸如：品種、成熟度、檢收時期、鮮果之貯藏、果實大小、季節及產地，以及加工條件及貯藏等。有鑑於果汁加工後獲得安定性，尋求適當之殺菌條件，將原料果汁在設定之 75°、80°、85°、90° 及 95°(±1)°C，40秒之加熱條件下，利用實驗型 VHX 板式熱交換機殺菌，均可完全達到滅菌。香氣、有機酸、糖類等則以 75°C 40秒加熱後立刻冷却凍藏者最安定，保留率也最高。顏色方面經加熱後均較未加熱之對照組爲暗，代表紅色的 $+a$ 值與代表黃色的 $+b$ 值均有降低之趨勢。黏度經加熱者均較對照組爲高，且經85°C，40秒加熱殺菌者黏度最高。就整個果汁品質之評估上，仍以 75°C，40秒鐘之殺菌條件最好，凍藏者較室溫貯藏者更爲安定。

葡萄 B_{2119} 色素之萃取及穩定性研究

黃淑雯　陳雪娥　冉祥偉

食品科學　第十三卷　第一、二期　第51-59頁　七十五年

葡萄 B_{2119} 的果肉及果皮中富含花青素，以不同的溶劑萃取之（包括含0.1% HCl 之乙醇，含 0.1% HCl 之甲醇、0.05% 偏磷酸水溶液及蒸餾水），比較其萃取效果。發現以 0.1% HCl 之乙醇萃取率最高。在色素穩定性方面，色素酒精液受到溫度的影響很大，溫度越低色素殘存率愈高，照光與否影響不明顯，添加維生素丙有促進色素減少的傾向，而充氮處理更加速此種現象。果汁中的色素則較於色素酒精液中不穩定，低溫（5°C）貯藏可延緩果汁中花青素的變化，但時間增長沈澱物增多，反而降低花青素的殘存量。色素粉末則以經離子交換樹脂處理的較未經處理的穩定性高，低溫貯藏及充氮處理對色素的保存有良好的效果，而光線則影響不大。

服　裝　配　色

胡　澤　民

家的組曲，書評書目出版社，75年4月，p. 56-59

服裝配色除了考慮衣服本身的色彩以外，還包括了整體性的膚色、髮型、體型、配件以及環境、場合、內在氣質、談吐風度等，都是服裝配色的重要條件。配色的基本原則有三種：㈠對比配色：利用色相、色調（色彩的明度與彩度）的對比變化、配合大小面積以及不同布料等特性，所產生的強調性與緩和性的對比效果。㈡調和配色：利用色相的明度漸序變化；或以近似色相互相搭配（如暖色

系、寒色系、中性色系）；也可運相同明度或彩度的不同顏色作爲配色的對象，所產生安定和諧的效果。㈢多色配色：有計畫地將色彩富於多種用途或任務，使色彩達到多樣變化的顯眼效果。一般布料可分爲單色素面布和多彩圖案的印花布，素色的衣服，可做多元性的組合配色，一件可化做多件穿着，經濟實惠；印花布給人的感覺，就好像多彩多姿的鮮花一樣，這些花紋圖案大致可分爲：散點、幾何、自然以及混合圖案四類；此外，由於布料的質地不同所產生的粗密、軟硬輕重、厚薄、凹凸、光澤與透明等變化，也都直接影響色彩的效果與表情，所以在配色經驗中，務必深入了解，並且充分掌握每個人的優點，如造型、品味、習慣等審愼地作適當的補足與强調。